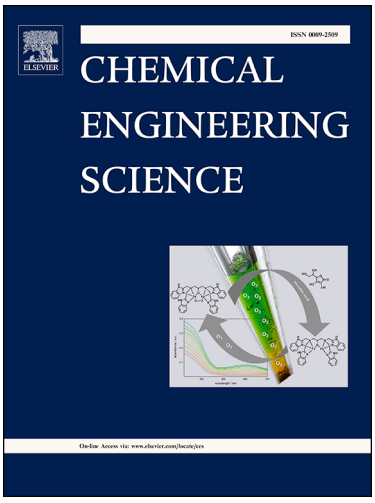

Sensitivity Analysis and Validation of a Two Fluid Method (TFM) model for a Spouted Bed

Cristina Moliner, Filippo Marchelli, Laura Ong, Alfonso Martinez-Felipe, Dominic Van der A, Elisabetta Arato

PII: S0009-2509(19)30506-8
DOI: https://doi.org/10.1016/j.ces.2019.06.008
Reference: CES 15029

To appear in: *Chemical Engineering Science*

Received Date: 6 March 2019
Revised Date: 7 May 2019
Accepted Date: 7 June 2019

Please cite this article as: C. Moliner, F. Marchelli, L. Ong, A. Martinez-Felipe, D. Van der A, E. Arato, Sensitivity Analysis and Validation of a Two Fluid Method (TFM) model for a Spouted Bed, *Chemical Engineering Science* (2019), doi: https://doi.org/10.1016/j.ces.2019.06.008

Sensitivity Analysis and Validation of a Two Fluid Method (TFM) model for a Spouted Bed

Cristina Moliner[1], Filippo Marchelli[2*], Laura Ong[3], Alfonso Martinez-Felipe[3], Dominic Van der A[4], Elisabetta Arato[1]

[1] University of Genova, Department of Civil, Chemical and Environmental Engineering, Via Opera Pia 15A, 16145 Genova (Italy)

[2] Free University of Bozen-Bolzano, Faculty of Science and Technology, Piazza Università 5, 39100 Bolzano (Italy)

[3] Chemical and Materials Engineering Group, School of Engineering, University of Aberdeen, King's College, Aberdeen (United Kingdom) AB24 3UE, UK

[4] Mechanics of fluids, soils and structures research group, School of Engineering, University of Aberdeen, King's College, Aberdeen (United Kingdom) AB24 3UE, UK

*Corresponding author: filippo.marchelli@natec.unibz.it

Abstract

A spouted bed has been simulated through a Computational Fluid Dynamic model using the Two Fluid Method and validated against experimental data. A sensitivity analysis has assessed the influence of the characteristic parameters on the solution. Among them, the accurate selection of the drag law seems to have the strongest influence on the results. In order to extend the capabilities of Ansys Fluent, Di Felice's drag law was also considered through a User Defined Function. The assessment of the granular phase and its kinetic, collisional and frictional forces, is highly relevant to achieve a correct prediction of the particle velocity profile. The specularity coefficient appears to be more influencing than the restitution coefficient, but both parameters are useful to optimise the model. Overall, the prediction of the particle vertical velocity is accurate whereas the height of the fountain is slightly over-predicted.

Keywords: computational fluid dynamics; two fluid model; multiphase flows; granular materials; Ansys Fluent.

1. INTRODUCTION

Spouted Beds (SB) were originally developed in the early 1950's as an alternative to conventional wheat driers that caused grain damage (Mathur and Gishler, 1955), because of the vigorous particle movement inside the reactors. Research then broadened towards the application of SB to achieve effective mixing and heat transfer in different solids and fluidising agents, including coarse and fine particles. Currently, SB are widely used in several industrial areas, such as, drying of grains (Brunello et al., 1974), coating (Chen and Kuo, 2015; Mollick et al., 2015), heterogeneous catalysis (Kechagiopoulos et al., 2007), gasification (Bove et al., 2018; Erkiaga et al., 2013), combustion (San José et al., 2014, 2013) and pyrolysis (Arregi et al., 2017; Makibar et al., 2015) of waste, among others. In a conventional SB, the fluid enters the vessel through a single central orifice plate, generating three well-differentiated zones: the channel created by the inlet fluid, (*spout*), the top of the bed of particles in continuous movement (*fountain*), and the space within the vessel surrounding the spout (*annulus*) (Mathur and Epstein, 1974). In short, particles rapidly move upwards in the spout and are dispersed radially outwards in the fountain, entering the annulus, where they slowly move downwards and radially inwards. Control and optimisation of the fluid dynamics in SB is paramount to achieve optimal operational results in the reactor (Cristina Moliner et al., 2017).

The continuous increase in computational power makes computer fluid dynamics a very attractive tool to reduce time and costs in the development of new SB technologies with multiphase flows. Two main modelling approaches are applied to simulate SB reactors: the two-fluid model (TFM) and the discrete element method (DEM). DEM tracks the particles composing the system, and is considered the most intuitive strategy for gas-solid flows. As the number of particles increases, however, the trajectory analysis becomes timely and computationally expensive. Alternatively, TFM models are much less computationally expensive than DEM, which makes them more viable at industrial scale. Even though several TFM models have been described for SB (Cristina Moliner et al., 2017), their accuracy is still insufficient and the choice of the main parameters (*i.e.* drag law, turbulence, solid stresses …) can considerably limit the results, particularly when interaction

between phases plays a major role. In this work, we have modelled a spout reactor through TFM, treating both solid and gas phases as interpenetrating continua.

The validation of new proposed numerical models requires experimental studies, which can reveal relevant information on the flow regimes (Yang et al., 2018), solids behaviour and mixtures (Moliner et al., 2018a), stability (Olazar et al., 1993) or scale up (He et al., 1997) of SB. Even though the particle behaviour can be easily observed from single experiments, complete sets of experimental data are rather limited in the literature (He et al., 1994a, 1994b; Liu et al., 2008), and some parameters are difficult to determine empirically (e.g. restitution or specularity coefficient), ultimately compromising the success of the CFD models (S.H. Hosseini, G. Ahmadi, B. S. Razavi, 2010). In this work, the experimental results obtained by Zhao et al. (Zhao et al., 2008) were taken as a reference to evaluate and validate our TFM model. The particle velocity distributions and particle flow patterns were determined by particle image velocity (PIV) in a pseudo-2D rectangular SB. Very recently, we described the validation of a DEM model (Marchelli F., Moliner C., Bosio B., 2019) using the same set of data, and in the present work we now apply the results to investigate on most of the characteristic parameters of our TFM model.

Simulations are performed using ANSYS Fluent 19.1, and the focus is on the selection of a suitable drag function as drag is the predominant force in SB, and the application of Di Felice's drag function by means of a User Defined Function (UDF), to gain design flexibility. Also, the definition of parameters regarding the solid phase is widely discussed through the application of the Kinetic Theory of Granular Flow (KTGF), including friction, kinetic and collisional distribution of forces. Finally, an optimised numerical model is proposed and validated.

2. NUMERICAL MODEL DESCRIPTION

TFM models use a generalised form of the Navier-Stokes equations, with each phase having independent properties. The fluid and solid phases are treated mathematically as interpenetrating continua and the volume fractions of the overlapping phases are assumed to be continuous functions of space and time. Equivalent conservation equations are used for each phase and

additional closure laws are applied to describe particle–fluid and particle–particle interactions, using the KTGF (Lun C.K.K., Savage S.B., Jeffrey D.J., 1984).

2.1. Governing equations

The continuity equation for each phase q (g - gas or s - solid) assuming no mass transfer between phases (*i.e.* no temperature effects or particle shrinking or swelling) is:

$$\frac{\partial}{\partial t}\left(\alpha_q \rho_q\right)+\nabla\left(\alpha_q \rho_q \vec{u}_q\right)=0 \qquad \text{Eq. 1}$$

where ρ_q and $\vec{u}_q$ are the density and velocity of phase q respectively and solid volume fraction is $\alpha_s = 1-\alpha_g$.

Similarly, the momentum equation for each phase *q* (q = g, s) is:

$$\frac{\partial}{\partial t}\left(\alpha_q \rho_q \vec{u}_q\right)+\nabla\left(\alpha_q \rho_q \vec{u}_q \vec{u}_q\right)=-\alpha_q \nabla p+\alpha_q \rho_q (\vec{g}+\vec{F}_q+\vec{F}_{lift,q}+\vec{F}_{vm,q})+\nabla \vec{\vec{\tau}}_q+\sum_{q=1}^{n}\vec{R}_{pq} \qquad \text{Eq. 2}$$

where p is the fluid pressure, $\vec{g}$ is the gravitational acceleration ($\vec{g}_z$ = -9.81 m/s^2), $\vec{F}_q$ is the external body acceleration, $\vec{F}_{lift,q}$ is the lift acceleration, $\vec{F}_{vm,q}$ is the virtual mass acceleration, $\vec{\vec{\tau}}_q$ is the Reynolds stress tensor and $\vec{R}_{pq}$ is the interaction force between phases.

Lift forces are considered when particle size is relatively large and account for the forces acting on a particle in response to velocity gradients in the air flow field. Virtual mass occurs when a solid phase accelerates relative to the gas phase. The influence of lift and virtual mass effects will be evaluated in Section 4.3.1.

The concept of granular temperature of the solids phase, $\Theta_s = \frac{u_s^2}{3}$, is introduced as a measure of particle velocity fluctuations, and the conservation equation for the granular phase *s* is given by:

$$\frac{3}{2}\left[\frac{\partial}{\partial t}\left(\alpha_s \rho_s \Theta_s\right)+\nabla\left(\alpha_s \rho_s \Theta_s\right)\vec{u}_s\right]=\left(-p_s \cdot \vec{\vec{I}}+\vec{\vec{\tau}}_s\right):\nabla \vec{u}_s-\nabla(k_{\Theta_s}\nabla\Theta_s)-\gamma_{\Theta_s}+\phi_s \qquad \text{Eq. 3}$$

with $\left(-p_s \cdot \vec{\vec{I}}+\vec{\vec{\tau}}_s\right):\nabla \vec{u}_s$: generation of energy by the solid stress tensor (p_s: solids pressure discussed in Section 4.3.5); $k_{\Theta_s}\nabla\Theta_s$: diffusion of energy; ϕ_s: energy exchange between the fluid

and solid phases ($\phi_s = -3\beta\Theta_s$) and γ_{Θ_s} : collisional dissipation of energy (Lun C.K.K., Savage S.B., Jeffrey D.J., 1984) (Eq. 4),

$$\gamma_{\Theta_s} = \frac{12(1-e_{ss}{}^2)\alpha_s^2\rho_s g_0 \Theta_s^{3/2}}{d_p\sqrt{\pi}} \quad \text{Eq. 4}$$

where e_{ss} is the inter-particle restitution coefficient, a measure of energy dissipation in particle-particle collisions (discussed in Section 4.3.8), and g_0 the radial distribution function, defined as a correction factor that modifies the probability of collisions between grains (discussed in Section 4.3.6).

2.2. Closure equations

2.2.1. Gas-solid interactions

The first set of closure equations regards the *gas-solid momentum exchange*, which defines the drag force exerted on particles in fluid-solid systems. These are usually expressed by the product of a momentum transfer coefficient β and the relative velocity ($\vec{u}_g - \vec{u}_s$) between the two phases. Literature shows a great number of tested several drag models in CFD-DEM simulations, which is not the case for TFM simulations. In particular, the vast majority of the simulation works have been performed with the Gidaspow drag model, followed by the Syamlal-O'Brien model (Cristina Moliner et al., 2017).

The momentum transfer coefficient is a key modelling parameter for the simulation of spouted beds and, given that SB present both dilute and dense zones, all the drag functions available within Fluent have been tested in Section 4.3.2 (Table 1). In addition, Di Felice's drag model (Di Felice, 1994) was included using a user-defined function (UDF), in which the gas-solid exchange coefficient was defined as:

$$\beta = \frac{3}{4}C_D\frac{\left(\alpha_g(1-\alpha_g)\rho_g|\vec{u}_g - \vec{u}_s|\right)}{d_p}\alpha^{-\eta} \quad \text{Eq. 5}$$

where η varies as a function of Re for fluidized bed systems, given as:

$$\eta = 3.7 - 0.65\exp[-\tfrac{1}{2}(1.5 - \log(\mathrm{Re}))^2] \quad \text{Eq. 6}$$

Drag on a single particle, $C_{D,}$ is determined from Dalla Valle's formula (Dallavalle, 1943) which is applicable across the practical range of Re, given as:

$$C_D = \left(0.63 + 4.8\sqrt{\frac{1}{\mathrm{Re}}}\right)^2 \quad \text{Eq. 7}$$

$$\mathrm{Re} = \frac{\rho_g d_p \alpha_g |\vec{u}_g - \vec{u}_s|}{\mu_g} \quad \text{Eq. 8}$$

Table 1. Overview of drag functions for fluid-solid interactions available within Fluent 19.1.

2.2.2 Solid phase

The challenge for TFM is to represent the solid phase accurately. The KTGF (Lun C.K.K., Savage S.B., Jeffrey D.J., 1984) is applied as an analogy to the well-established kinetic theory of gases, in order to calculate the *solid-solid momentum exchange* through the solids shear stress interfacial forces, as well as turbulence in both phases.

Two flow regimes can be distinguished in granular flows. At *high particle concentrations* (bed of the reactor) individual particles interact with the multiple neighbours and normal and tangential *frictional forces* ($\mu_{s,fr}$) are the major contributions on the particle stresses. At *low particle concentrations*, on the other hand, stresses are mainly caused by particle-particle *collisions* ($\mu_{s,col}$) or translational transfer of momentum ($\mu_{s,kin}$) (Campbell, 2006). The kinetic theory takes both approaches and considers the sum of a rapidly shearing flow regime, in which kinetic contributions are dominant, and a quasi-static flow regime, in which friction is the dominant phenomenon. As a consequence, the solids shear (μ_s) viscosity can be calculated as:

$$\mu_s = \mu_{s,fr} + \mu_{s,col} + \mu_{s,kin} \quad \text{Eq. 9}$$

The frictional viscosity ($\mu_{s,fr}$) is given by Schaeffer et al. (G., 1987):

$$\mu_{s,fr} = \frac{p_s \sin\delta}{2\sqrt{I_{2D}}} \quad \text{Eq. 10}$$

with δ the angle of friction of particles equal to 28.5° for glass beads (Johnson P.C., Nott P., 1990). In this work, the effect of the minimum value of the solid phase fraction at which the frictional stress model becomes effective is investigated in Section 4.3.4.

The collisional contribution ($\mu_{s,col}$) of the shear viscosity is given by:

$$\mu_{s,col} = \frac{4}{5}\alpha_s^2 \rho_s d_s g_0 (1+e_{ss})\sqrt{\frac{\Theta_s}{\pi}} \quad \text{Eq. 11}$$

The kinetic contribution ($\mu_{s,kin}$) can be modelled by the Gidaspow (GID) (Gidaspow et al., 1992) and Syamlal O'Brien (SOB) (M. Syamlal, W. Rogers, 1993) expressions, which will be evaluated in Section 4.3.7.

GID

$$\mu_{s,kin} = \frac{10\rho_s d_s \sqrt{\pi\Theta_s}}{96(1+e_{ss})g_0}\left[1+\frac{4}{5}g_0\alpha_s(1+e_{ss})\right]^2 \quad \text{Eq. 12}$$

SOB

$$\mu_{s,kin} = \frac{\alpha_s \rho_s d_s \sqrt{\pi\Theta_s}}{6(3-e_{ss})}\left[1+\frac{2}{5}g_0\alpha_s(1+e_{ss})(3e_{ss}-1)\right] \quad \text{Eq. 13}$$

Finally, the solids bulk viscosity (λ_s), which accounts for the resistance of granular particles to compression and expansion, is given as (Lun C.K.K., Savage S.B., Jeffrey D.J., 1984):

$$\lambda_s = \frac{4}{3}\alpha_s \rho_s d_s g_0 (1+e_{ss})\left(\frac{\Theta_s}{\pi}\right)^2 \quad \text{Eq. 14}$$

3. MODEL SET UP

3.1. Definition of the device geometry and mesh

The experimental apparatus described in Zhao et al. (Zhao et al., 2008) was used in all simulations through representation of the original experimental device (depth = 0.015 m). The schematic view of the geometry and its dimensions are presented in Figure 1a, and further details on the

experimental conditions can be found in (Zhao et al., 2008). The physical characteristics of the solids and air are summarised in Table 2.

Various mesh sizes defined by the number of divisions per edge (*i.e.* 30, 40 and 55), along the conical and straight edges above the inlet tube, were tested. The divisions are in the y-direction, as shown on the mesh in Figure 1b.

Figure 1. Main dimensions of the simulated spouted bed (a) and definition of coarse mesh (b)

Table 2. Definition of experimental conditions

3.2. Initial and boundary conditions

The bed was composed of glass beads (Geldart – Group D), and was initially considered as a static bed (t = 0 s). Its initial height was set at 0.1 m with the particles placed evenly patched all over the domain with α_s = 0.63. Uniform air at room temperature is used as fluidising agent, with an inlet velocity of 26.68 m/s along the *z* axis. The flow is assumed to be fully developed in the free-board (i.e. area above the fountain). A non-slip boundary condition at the lateral bed wall is assumed for the gas phase. The influence of the solid-wall interaction at different specularity coefficients (φ = 0.05-0.99) will be evaluated in Section 4.3.9

3.3. Physical models

The governing equations were implemented through the *Multiphase model*. Two Eulerian phases were considered, including a granular phase (glass beads). The turbulent gas fluctuations in the spout and annulus might have an influence on the gas-solid behaviour. However, there is no consensus on whether turbulence should be taken into account or not (C. Moliner et al., 2017). In the present simulations, turbulence was considered using the k-ε dispersed model with a scalable wall function as suggested by (ANSYS, 2018a) reinforced by our previous studies (Marchelli et al.,

2019). A description of equations and coefficients can be found in the Supplementary material. The phase-coupled SIMPLE algorithm was applied for the pressure-velocity coupling with the discretisation schemes as described in (Moliner et al., 2018b).

A complete sensitivity analysis was carried out as follows: first, an initial set of reference parameters was defined on the basis of previous simulations (Moliner et al., 2018b). Table 3 lists the reference and tested options for all the studied parameters. Then, sensitivity analyses were performed by changing the individual parameters, while maintaining the rest constant.

Table 3. Initial reference parameters and tested options for all the varied parameters

The influence of lift (L) and virtual mass (VM) on the results was firstly studied, followed by drag (DL) and granular temperature (Θ_s). Successively, the granular phase was analysed in detail. Frictional, kinetic and collisional stresses were analysed in depth: the threshold for the activation of the Schaeffer friction model was firstly assessed (FPL) followed by the study of collisional (p_s, g_0) and kinetic forces (GV). Finally, the parameters for the particle-particle (e_{ss}) and particle-wall (φ) interactions were used to optimise the model by fitting to the experimental data.

All simulations started from a static bed condition. In the experiments quasi-steady state was achieved after about 0.5s. In the present simulations the simulation was run for 0.6s, after which the simulation was ran for another full second with the unsteady statistics calculation activated in order to obtain the time-averaged quantities. In addition, 30 s of simulated time using the optimized solution confirmed the stability of the system during that period. The simulations were carried out using a PC Intel® Core™ i5-5200U CPU 540 @2.2GHz and 8GB RAM.

Simulated results were compared with the experimental results obtained by Zhao et al (Zhao et al., 2008). The height of the fountain, H_F, and maximum velocity of solids along the axial height, v_{zmax},

were taken as representative values to quantify the difference between simulated and experimental data:

- v_{zmax} = 1.013 m/s, calculated as the velocity after which the particles initiate to decelerate due to the formation of the fountain.
- H_F = 0.135 m, calculated as the height at which the velocity of particles is zero.

4. RESULTS AND DISCUSSION

4.1. Mesh independence test

The grid independence is of key importance to obtain reliable models of multiphase flows. The simulation results using the reference parameters (Table 3) were compared for three different mesh sizes. Figure 2 shows the particle velocity in the axial direction for coarse (7680 cells), medium (9920 cells) and fine (13280 cells) grids. Medium and fine meshes result in identical results while the coarse grid shows a discrepancy with the other grids. Therefore, the medium size was selected to achieve a compromise between accuracy and time of calculation.

Figure 2. Effect of grid sizes on the particles vertical velocity profile along axial height.

4.2. Validation of the User Defined Function (UDF)

The User Defined Function (UDF) was tested with the already implemented in Fluent Wen-Yu (WY) model due to the similarity with Di Felice's. The UDF firstly computes Re, followed by C_D, and the corresponding η for WY or Di Felice. In cases where α_g or $|\vec{u}_g - \vec{u}_s|$ is zero, Re and β are also zero, and the computed C_D returned an error as it is a function of $\frac{1}{\mathrm{Re}}$. As β is zero in these cases, the value of C_D has no effect and therefore can be assumed as zero to prevent errors in the execution of the UDF. Figure 3 shows the validation of the UDF for WY.

Figure 3. Verification of UDF using WY drag model

4.3. Sensitivity analysis

4.3.1. Lift and virtual mass forces

By definition, lift forces are caused by the shearing effect of fluids onto particles, and virtual mass effects by relative accelerations between phases. In general, lift (L) and virtual mass (VM) forces can be neglected when simulating fluidised beds as the predominant forces are gravity and drag effects (ANSYS, 2018b). Prior to the sensitivity analysis, this possibility was tested using the reference settings (Table 3). Figure 4 shows the averaged particle vertical velocity along the spout centreline (4a) and the lateral particles vertical velocity at a height of z = 91.2 mm from the inlet (4b). The simulations confirm that it is possible to neglect lift and virtual mass forces (NO L/VM) as they provide identical results. As a consequence, Eq. 2 results in the following simplified expression:

$$\frac{\partial}{\partial t}\left(\alpha_q \rho_q \vec{u}_q\right) + \nabla\left(\alpha_q \rho_q \vec{u}_q \vec{u}_q\right) = -\alpha_q \nabla p + \alpha_q \rho_q \vec{g} + \nabla \vec{\bar{\tau}}_q + \sum_{q=1}^{n} \vec{R}_{pq} \qquad \text{Eq. 15}$$

These results are in partial accordance with our previous work in which DEM was used to simulate the same experimental data, where Saffman lift forces had a negligible influence on the solution (Marchelli F., Moliner C., Bosio B., 2019). We found however that Magnus lift did provide differences on the results. In any case, this force is based on the rotation of particles and so it cannot be included in TFM which could be a source of discrepancies between experimental data.

Figure 4a shows the different areas within the spouted bed. The particles accelerate rapidly in the inlet until achieving a constant velocity at the top of the spout. The maximum velocity used for quantitative calculations is taken as the value after which the particles start to decelerate when they form the fountain. The height of the fountain, H_F, is calculated as the position in which the vertical velocity of particles is zero. Below H_F, particles descend through the annulus until they are recaptured by the spout, initiating the cycle again. In Figure 4b, particle velocity reaches its maximum at the centre of the spout and decreases when moving outwards. The radius of the spout can be then calculated as the value for which the velocity of particles is zero, which represents the interface between the spout and the annulus.

Figure 4. Comparison of results considering (Ref.) and neglecting (NO L/VM) lift and virtual mass forces: (a) Vertical profile of particle velocity along axial height; (b) Lateral profile at bed level of 91.2 mm from inlet.

4.3.2. Drag function

The interphase momentum transfer between the solid and gas phase through the drag force is a key modeling parameter for the simulation of gas–solid systems. The drag law (DL), which has a primary effect on the interactions of the phases in spouted beds, has been studied in detail. The functions proposed by Syamal-Obrien (SOB), Di Felice (DF), Wen-Yu (WY), Gibilaro (GIB), Gidaspow (GID) and Huiling - Gidaspow (HG) were tested. All the expressions were already present in Ansys Fluent 19.1 (see (ANSYS, 2018b) for their complete mathematical description) except for DF, which was included through a UDF (see Section 4.2).

Figure 5 shows the averaged longitudinal profile of particle vertical velocity on the spout centreline (5a) and lateral particle vertical velocity in the spout at a bed level of 91.2 mm (5b), together with their comparison with the experimental data (squares). The influence of the drag function on the results is evident: some expressions describe well the particle vertical velocity (SOB, DF, the latter especially for the lateral profile), while others (WY, GIB) lie far from the experimental values. SOB and DF provide the best fitting of v_{zmax}, but fail to predict H_F, which is over-estimated. On the other hand, WY and GIB provide the best results in the fountain zone. In this case, simulations slightly over-predict H_F but considerably under-predict v_{zmax}.

Figure 5. Comparison of various drag models: (a) vertical profile along spout axis; (b) lateral profile at a bed level of 91.2 mm from the inlet.

Figure 6 shows the averaged contour plot of solids volume fraction using different drag laws, which result in different shapes for the spout and the fountain. WY and GIB present a more concentrated

spout but particles fall back rapidly, resulting in lower fountain heights than other models. The v_{zmax} and H_F parameters obtained using these models are compared to the experimental values in Table 4. As mentioned above, the lowest error in the prediction of v_{zmax} (axial direction) is obtained using SOB (0.4%), whereas H_F is better represented by GIB or WY. However, these cannot explain accurately the profile of the particle velocity, and are discarded for the simulations. Considering a compromise between accuracy in v_{zmax} and H_F, we propose SOB as the most suitable drag function (total error = $Error_1$ + $Error_2$ = 18.2%).

Figure 6. Averaged contour plot of solid volume fraction using different drag laws (DL).

Table 4. Simulation results and error (with respect to experimental data) for different DL.

The behaviour of some of these drag laws in CFD-DEM simulations was not completely similar (Marchelli F., Moliner C., Bosio B., 2019). The WY drag force provided the lowest fountain height, followed by the GID and SOB models, in excellent agreement with our own results. On the other hand, the maximum vertical velocity was almost the same when applying the WY and GID models, while it was quite higher with the SOB model. It is important to highlight that the drag function depends on the particle size, distribution and shape. For this work and according to the experimental data, particles were considered as uniform perfect spheres, and therefore these effects were neglected.

4.3.3. Granular temperature

The granular temperature (Θ_s in Eq. 3) is a measure of the particle velocity fluctuation calculated by the KTGF. It is highly related to the concentration of solids in the different SB zones: higher in the spout, intermediate in the fountain and lower in the annulus. Figure 7a and 7b show the longitudinal and lateral profiles of the particle vertical velocity, respectively, considering the algebraic and full transport equations for Θ_s. The use of the algebraic expression has proved to improve convergence and stability of the solution (Hosseini et al., 2013), and from the comparison

with experimental data, it is evident that it provides a better fitting in both cases. This means that convective and diffusion terms can be neglected, resulting in generation and dissipation terms being balanced (*i.e.* granular energy is dissipated locally).

Figure 7. Comparison of Θ_s models: (a) vertical profile along the spout axis; (b) lateral profile at bed level of 91.2 mm from inlet.

Figure 8 shows the contour plot of the averaged solid volume fractions obtained for the algebraic (a) and full transport (b) expressions. Different solid profiles are observed, and higher solids concentration is obtained in the fountain using the algebraic expression compared to the full transport equation. Despite this difference, both expressions result in similar H_F with slightly higher values for the full equation (at a fixed restitution coefficient value, in this case equal to 0.9), which is consistent to previous works (Hosseini et al., 2013).

Figure 8. Contour plot of averaged solid volume fractions for the algebraic (a) and full transport (b) expressions.

The algebraic expression was then taken as the optimal setting and thus Eq. 3 can be simplified as:

$$0 = \left(- p_s \cdot \vec{\vec{I}} + \vec{\vec{\tau}}_s \right) : \nabla \vec{u}_s - \gamma_{\Theta_s} \qquad \text{Eq. 16}$$

4.3.4. Friction Packing Limit

Gravity and drag forces are dominant for the majority of multiphase flows but, in the case of very dense ones, frictional stresses become significant and need to be taken into account. In the case of SB, particles in the annulus region undergo frictional contact with multiple neighbours due to the high solid volume fraction. Kinetic theory assumes binary and instantaneous collisions between particles, but when the solids concentration is high, it fails to describe the granular flow adequately. A suitable model is required not only in the annulus, but also in the spout zone (a dilute particulate region) in order to predict the spouted bed fluid dynamics. We then include an analysis of the frictional stress (Dan et al., 2010; Huilin et al., 2004) with the aim to overcome, at least to some extent, the absence of factors such as stick, glide and limit friction, or rotation forces, which are present in DEM but neglected in TFM.

Different values of minimum concentration for the transition point (FPL) were used to specify the threshold volume fraction at which the frictional regime becomes effective. Reducing FPL implies the inclusion of the frictional stresses for the particulate phase at lower concentrations. The minimum value of FPL = 0.5 was empirically proposed by Johnson and Jackson (Johnson P., 1987). Figure 9 shows the vertical profile along axial height at different FPL. It can be seen that Schaeffer's frictional stress model with FPL = 0.5 leads to a slight under-prediction of v_{zmax} and a correct velocity profile in the upper part of the spout, while the use of FPL = 0.57 over-predicts the entire profile. The high disagreement showed by FPL = 0.6 corroborates that frictional forces need to be present at low solid concentrations.

The stability of the bed is highly influenced by FPL. Figure 10 shows that, at a low values (FPL = 0.5) steady spouting is reached, in contrast with higher values (FPL = 0.6), which result in spout instabilities. Finally, lower FPL increases granular temperature in the spout and fountain due to frictional forces in dilute zones. The maximum values of granular temperature were found in the spout region (Figure 11), ranging from Θ_s = 0.0966 m^2/s^2 at FPL = 0.5 to Θ_s = 0.0956 m^2/s^2 at

FPL = 0.57. Given that the predictions of H_F are not influenced by this parameter, FPL = 0.55 was selected as optimum value due to its high agreement with the experimental particle velocity profile.

Figure 9. Comparison of FPL for the averaged particle vertical velocity along the axial height.

Figure 10. Contour plots for the averaged solids volume fraction at high and low FPL.

Figure 11. Granular temperature at different FPL.

4.3.5. Solid pressure

The solid pressure (p_s in Eq. 3) represents the pressure exerted on the spouted wall due to the presence of particles, and measures the momentum transfer by the motion of particles. It is assumed to play an important role in the granular phase, but there is not a clear consensus on the best expression for SB. Hence, different expressions were tested in the present simulations:

Lun et al.(Lun C.K.K., Savage S.B., Jeffrey D.J., 1984):

$$p_s = \alpha_s \rho_s \Theta_s \left[1 + 2 g_0 \alpha_s (1 + e_{ss})\right] \quad \text{Eq. 17}$$

SOB et al. (M. Syamlal, W. Rogers, 1993):

$$p_s = 2 \alpha_s^2 \rho_s (1 + e_{ss}) g_0 \Theta_s \quad \text{Eq. 18}$$

Ma-Ahmadi (Ahmadi, 1990):

$$p_s = \alpha_s \rho_s \Theta_s \left[(1 + 4 \alpha_s g_0) + \tfrac{1}{2}\left[(1 + e_{ss})(1 - e_{ss} + 2\mu_{s,fr})\right]\right] \quad \text{Eq. 19}$$

Figure 12 shows the averaged particle vertical velocity in the axial (12a) and lateral (12b) direction using the previous p_s expressions. LUN and SOB provide the most accurate representations for the particle vertical velocity profiles, and, among these, the SOB prediction for H_F is better, although slightly over-estimated. The main difference between the p_s expressions is the definition of the frictional viscosity, which is derived from the frictional pressure in the case of LUN and SOB,

and it is explicitly included in AHMADI expression. The derived equation depends on the solids distribution inside the bed and not on the particle properties (static, dynamic or rotational properties), whose effect becomes more important in dense beds. These limitations could be overcome when using a DEM approach, as it contains parameters defining the main characteristics of solids. The error between simulated and experimental results for v_{zmax} and H_F were also calculated in Table 5, and these results sustained the selection of SOB to describe p_s.

Figure 12. Comparison of p_s models: (a) vertical profile along axial height; (b) lateral profile at bed level of 91.2 mm from inlet.

Table 5. Simulated results and error with respect to experimental data for the tested p_s

4.3.6. Radial distribution

The radial distribution (g_0 in Eq. 4) specifies a correction factor that modifies the probability of collisions between grains when the solid granular phase becomes dense. Several expressions for g_0 were tested:

Lun et al. (S. Ogawa, A. Umemura, 1980)
$$g_0 = \left[1 - \left(\frac{\alpha_s}{\alpha_{s,\max}}\right)^{1/3}\right]^{-1} \quad \text{Eq. 20}$$

SOB (M. Syamlal, W. Rogers, 1993):
$$g_0 = \frac{1}{1-\alpha_s} \quad \text{Eq. 21}$$

Ma-Ahmadi (Ahmadi, 1990):
$$g_0 = \frac{1 + 2.5\alpha_s + 4.59\alpha_s^2 + 4.52\alpha_s^3}{\left[1 - \left(\frac{\alpha_s}{\alpha_{s,\max}}\right)^3\right]^{0.678}} \quad \text{Eq. 22}$$

Arastoopour (Iddir and Arastoopour, 2005):
$$g_0 = \left[1 - \frac{\alpha_s}{\alpha_{s,\max}}\right]^{-1} \quad \text{Eq. 23}$$

With $\alpha_{s,\max}$ the maximum packing limit equal to 0.63

Figure 13 shows the averaged particle vertical velocity in the axial (a) and lateral (b) direction using different expressions for g_0. As in the previous section, LUN and SOB provide the most accurate representation for the particle velocity profile, with SOB predicting better the H_F. Once again, the error between simulated and experimental results for v_{zmax} and H_F was calculated, see Table 6, suggesting that LUN was the best expression to describe g_0. Indeed, the empirical expression by LUN is recommended by Fluent's user guide (ANSYS, 2018b.) for multiphase systems with one solid phase.

Figure 13. Comparison of various g_0 models: (a) vertical profile along axial height; (b) lateral profile at bed level of 91.2 mm from inlet.

Table 6. Simulated results and error with respect to experimental data for the tested g_0

4.3.7. Granular viscosity

The granular viscosity (GV) represents the solids shear viscosity that arises due to kinetic ($\mu_{s,kin}$) and collisional ($\mu_{s,col}$) interactions of particles. Two different expressions, SOB and GID, were tested for the description of the kinetic part of the viscosity (see Section 2.2), and the corresponding results for the averaged particle vertical velocity are summarised in Figure 14 (see Eq. 12-13). Both expressions over-estimate H_F, but SOB deviates more considerably, hence we conclude that GID describes better the particles velocity profile in this case. This indicates a lower resistance of solids against their upward movement in the spout region, which is consistent with other works (Hosseini et al., 2013) that report lower GV values at low volume fractions.

Figure 14. Comparison of various GV: (a) vertical profile along axial height; (b) Lateral profile at bed level of 91.2 mm from inlet.

4.3.8. Restitution coefficient

The restitution coefficient (e_{ss} in Eq. 4) is a measure of the energy dissipation due to inelastic particle-particle collisions, and its value ranges from zero to unity, where e_{ss} = 1 indicates a perfectly elastic collision (*i.e.* no loss of relative velocity of the particle). e_{ss} depends on the particle's material, size, shape and roughness and it is difficult to calculate experimentally. It is equivalent to the dashpot term (η) in DEM models (Marchelli et al., 2017) and in both cases glass particles are known to be well described by high e_{ss} values (Hosseini et al., 2015, 2010; Rong and ZHAN, 2010).

Figure 15 shows the averaged particle vertical velocity in the axial (a) and lateral (b) direction using different e_{ss} values. Large differences in v_{zmax} and H_F are only observed for e_{ss} = 0.99, which is indicative of a low sensitivity of this parameter on the results. At higher e_{ss} values, the particle vertical velocity and fountain height decrease, due to the increase in the concentration of solids in the spout and fountain (Hosseini et al., 2013).

Figure 15. Comparison of e_{ss}: (a) vertical profile along axial height; (b) lateral profile at bed level of 91.2 mm from inlet.

Figure 16 shows the averaged contour plot of the concentration of solids as a function of e_{ss}, and Table 7 the calculated errors between simulated and experimental results for v_{zmax} and H_F. A more regular circulation of solids is obtained at low e_{ss} values, together with a more symmetric shape of the fountain is observed. Θ_s is also influenced by e_{ss}, as shown in Figure 17. Results range from Θ_s = 0.0961 m^2/s^2 at e_{ss} =0.9; to Θ_s = 0.0999 m^2/s^2 at e_{ss} =0.99. High values of e_{ss} lead to the

increase in Θ_s (*i.e.* increased particle-phase turbulence) and their related properties (solids pressure and granular viscosity), thereby increasing the loss of particle momentum, which in turn promotes lower particle velocity. Although the highest coefficient provided the most accurate prediction of HF, it failed to describe well the velocity profile, and therefore e_{ss} = 0.95 was taken as the optimal value. In DEM simulations (Marchelli F., Moliner C., Bosio B., 2019), the influence of the restitution coefficient (η) was found to be more straightforward, and v_{zmax} and H_F simultaneously decreased when η increased, with no signs of instability even at high η values.

Figure 16. Averaged contour plot of the concentration of solids at different e_{ss}.

Figure 17. Influence of e_{ss} on Θ_s.

Table 7. Simulated results and error with respect to experimental data for the tested e_{ss}

4.3.9. Specularity coefficient

Particle-wall interactions can be modelled by using the specularity coefficient (φ) (T. Li, J. Grace, 2010), which is defined as the average fraction of relative tangential momentum transfer during a particle-wall collision (Johnson P.C., Nott P., 1990). φ is an indicator of the smoothness of the wall, and it ranges from zero to unity, where $\varphi = 0$ indicates a perfectly specular collision against a smooth wall, and $\varphi = 1$ a totally diffuse collision against a rough wall. The selection of φ is usually not known *a priori* and, as in the case of e_{ss}, it is difficult to determine experimentally (M.V.C. Machado, S.M. Nascimento, C.R. Duarte, 2017). Figure 18 shows a quantitative comparison of the effect of φ on the particle velocity along the spout centreline. The results at φ < 0.8 show similar particle velocity profiles and very accurate predictions of v_{zmax}, but higher values describe more precisely the whole range of particle velocities. Moreover, the prediction of H_F is highly influenced by φ, where lower values result in higher H_F.

Figure 18. Effect of φ on the vertical profile along axial height

The influence of φ is more evident than e_{ss} (see Figure 15), suggesting that the inelasticity of particle-wall collisions might be more relevant than particle-particle collisions in our model (Golshan et al., 2017). The error between simulated and experimental results for v_{zmax} and H_F was calculated as a function of φ, and the results are listed in Table 8. Even though φ = 0.7 provides the exact prediction of v_{zmax}, the optimal specularity coefficient is taken as 0.99 as it presents the lowest total error (error = 13%).

Figure 19. Contour plot of solids volume fraction at different φ.

Table 8. Simulated results and error with respect to experimental data for the tested φ.

It is important to highlight that the specularity coefficient is highly affected by the geometry of the simulated object (*i.e.* 2-D or 3-D). The good agreement using high φ, implies low dissipation of granular energy at the wall. In 2-D simulations, the effect of the particle collisions with the back and front walls are not considered, resulting in over-predicted H_F values. In the present simulations, the geometry reproduced exactly the experimental apparatus (pseudo 2-D) and thus a limited effect of the walls might be present.

5. Optimised solution

We now present a final simulation considering all the optimal values obtained in Section 4, and the averaged particle vertical velocity along the spout centreline (a) and lateral (b) profile at a bed level of 91.2 mm from the inlet (b), is shown in Figure 20. The circulation of particles and the air velocity within the SB can be clearly seen form Figure 21.

The particles are entrained from the annulus into the gas stream near the entrance region surrounding the gas inlet, and then move upward within the spout region by the gas drag force. The particles rise into the fountain, and finally fall down onto the annulus completing the cycle. It is interesting to note that the predicted value of particle velocity in the spout is approximately 10 times higher than that in the annulus, which is in great agreement with the experimental data (Zhao et al., 2008). Also, the partition of the gas flow into spout and annulus affects the efficiency of the gas-solid contact. Although the optimised model provides a good prediction of the velocity profile, the height of the fountain is still over-predicted (H_F = 0.150 m). The same difficulty was also encountered in the optimisation of the CFD-DEM model (Marchelli F., Moliner C., Bosio B., 2019).

Figure 20. Comparison of the optimised solution (line) and experimental data (squares): (a) vertical profile along axial height; (b) lateral profile at bed level of 91.2 mm from inlet.

Figure 21. Simulated flow fields of particles (a) and air (b) in the SB.

It is clear that these results might obviously not be identically applicable to different geometries, gas velocities and particles, but they can represent a valid starting point to optimise a CFD-TFM model.

6. CONCLUSIONS

A spouted bed (SB) has been simulated using the TFM Computational Fluid Dynamic model, which has been validated against experimental data. Overall, the prediction of the particle vertical velocity is accurate (error of optimised solution = 0.1 %) whereas the height of the fountain is over-predicted (error of optimised solution = 11 %). A sensitivity analysis has assessed the influence of the characteristic parameters on the solution. Among them, the accurate selection of the drag law

seems to have the strongest influence on the results, whilst the assessment of the granular phase and its kinetic, collisional and frictional forces, is highly relevant to achieve a correct prediction of the particle velocity profile. The specularity coefficient (optimised value = 0.99) appears to be more influencing than the restitution coefficient (optimised value = 0.95), but both parameters are useful to optimise the model.

Nomenclature

C_D	drag coefficient [-]
d_p	particle diameter [mm]
e_{ss}	particle-particle restitution coefficient [-]
$F_{lift,q}$	lift acceleration [m/s^2]
F_q	external body acceleration [m/s^2]
$F_{vm,q}$	virtual mass acceleration [m/s^2]
g	gravitational acceleration [m/s^2]
g_0	radial distribution function [-]
H_F	height of the fountain [m]
I	identity tensor [-]
$k_{\Theta s}$	diffusion coefficient for the granular energy [kg/(m·s)]
m	mass of a particle [kg]
p	pressure [Pa]
R_{pq}	interaction force between the gas and solid phases [N/m^3]
Re	Reynolds number [-]
u	phase velocity [m/s]
v_z	particle vertical velocity [m/s]

Greek Symbols

α	volume fraction [-]
α_{max}	maximum packing limit [-]
β	gas-solid exchange coefficient [kg/(m^3·s)]
$\gamma_{\Theta s}$	collisional dissipation of energy [Pa/s]
Θ_s	granular temperature [m^2/s^2]
λ_s	solids bulk viscosity [Pa·s]
μ	dynamic viscosity of the fluid [Pa·s]
μ_s	solids shear viscosity (fr-frictional, col-collisional, kin-kinetic) [Pa·s]
ρ	density [kg/m^3]
τ_s	Reynolds stress tensor [Pa]
φ	specularity coefficient [-]

Subscripts

g	relative to the gas phase
p	particle
q	generic continuum phase
s	relative to the solid phase

6. BIBLIOGRAPHY

Ahmadi, D.M. and G., 1990. A Thermodynamical Formulation for Dispersed Multiphase Turbulent Flows. Int. J. Multiph. Flow 16, 323–351.

ANSYS, 2018a. Chapter 4: Turbulence, in: Fluent Theory Guide. ANSYS, Inc.

ANSYS, 2018b. Chapter 17: Multiphase Flows, in: ANSYS FLUENT Theory Guide. ANSYS.

Arregi, A., Amutio, M., Lopez, G., Artetxe, M., Alvarez, J., Bilbao, J., Olazar, M., 2017. Hydrogen-rich gas production by continuous pyrolysis and in-line catalytic reforming of pine wood waste and HDPE mixtures. Energy Convers. Manag. 136, 192–201. https://doi.org/10.1016/j.enconman.2017.01.008

Bove, D., Moliner, C., Curti, M., Baratieri, M., Bosio, B., Rovero, G., Arato, E., 2018. Preliminary Tests for the Thermo-Chemical Conversion of Biomass in a Spouted Bed Pilot Plant. Can. J. Chem. Eng. https://doi.org/10.1002/cjce.23223

Brunello, G., Peck, R.E., Nina, G. Della, 1974. The drying of barley malt in the spouted bed dryer. Can. J. Chem. Eng. 52, 201–205. https://doi.org/10.1002/cjce.5450520211

Campbell, C.S., 2006. Granular material flows – An overview. Powder Technol. 162, 208–229. https://doi.org/10.1016/j.powtec.2005.12.008

Chen, W.Y., Kuo, H.P., 2015. Surface coating of group B iron powders in a spouted bed. Procedia Eng. 102, 1144–1149. https://doi.org/10.1016/j.proeng.2015.01.238

Dallavalle, J.M., 1943. Micromeritics: The technology of fine particles. Pitman Publishing Corporation.

Dan, S., Shuyan, W., Gougdong, L., Shuai, W., Yongjian, L., Lixin, W., 2010. Simulations of flow behavior of gas and particles in a spouted bed using a second-order moment method-frictional stresses model. Chem. Eng. Sci. 65, 2635–2648. https://doi.org/10.1016/j.ces.2009.12.042

Di Felice, R., 1994. The voidage function for fluid-particle interaction systems. Int. J. Multiph. Flow 20, 153–159. https://doi.org/10.1016/0301-9322(94)90011-6

Erkiaga, A., Lopez, G., Amutio, M., Bilbao, J., Olazar, M., 2013. Steam gasification of biomass in a conical spouted bed reactor with olivine and ??-alumina as primary catalysts. Fuel Process. Technol. 116, 292–299. https://doi.org/10.1016/j.fuproc.2013.07.008

G., S., 1987. Instability in the evolution equations describing incompressible granular flow. J. Differ. Equations 66, 19–50.

Gidaspow, D., Bezburuah, R., Ding, J., 1992. Hydrodynamics of Circulating Fluidized Beds, Kinetic Theory Approach, in: Fluidization VII - Proceedings of the 7th Engineering Foundation Conference on Fluidization. pp. 75–82.

Golshan, S., Zarghami, R., Mostoufi, N., 2017. Hydrodynamics of slot-rectangular spouted beds: Process intensification. Chem. Eng. Res. Des. 121, 315–328. https://doi.org/10.1016/j.cherd.2017.03.022

He, Y.-L., Lim, C.J., Grace, J.R., 1997. Scale-up studies of spouted beds. Chem. Eng. Sci. 52, 329–339. https://doi.org/10.1016/S0009-2509(96)00378-8

He, Y.-L., Lim, C.J., Grace, J.R., Zhu, J.-X., Qzn, S.-Z., 1994a. Measurements of voidage profiles in spouted beds. Can. J. Chem. Eng. 72, 229–234. https://doi.org/10.1002/cjce.5450720208

He, Y.-L., Qin, S.-Z., Lim, C.J., Grace, J.R., 1994b. Particle velocity profiles and solid flow patterns in spouted beds. Can. J. Chem. Eng. 72, 561–568. https://doi.org/10.1002/cjce.5450720402

Hosseini, S.H., Ahmadi, G., Olazar, M., 2013. CFD simulation of cylindrical spouted beds by the kinetic theory of granular flow. Powder Technol. 246, 303–316. https://doi.org/10.1016/j.powtec.2013.05.016

Hosseini, S.H., Ahmadi, G., Saeedi Razavi, B., Zhong, W., 2010. Computational fluid dynamic simulation of hydrodynamic behavior in a two-dimensional conical spouted bed. Energy and

Fuels 24, 6086–6098. https://doi.org/10.1021/ef100612r

Hosseini, S.H., Fattahi, M., Ahmadi, G., 2015. Hydrodynamics studies of a pseudo 2D rectangular spouted bed by CFD. Powder Technol. 279, 301–309. https://doi.org/10.1016/J.POWTEC.2015.04.013

Huilin, L., Yurong, H., Wentie, L., Ding, J., Gidaspow, D., Bouillard, J., 2004. Computer simulations of gas-solid flow in spouted beds using kinetic-frictional stress model of granular flow. Chem. Eng. Sci. 59, 865–878. https://doi.org/10.1016/j.ces.2003.10.018

Iddir, H., Arastoopour, H., 2005. Modeling of multitype particle flow using the kinetic theory approach. AIChE J. 51, 1620–1632. https://doi.org/10.1002/aic.10429

Johnson P., C.J.R., 1987. Frictional-collisional constitutive relations for granular materials with applications to plane shearing. J. Fluid. Mech. 176, 67–93.

Johnson P.C., Nott P., J.R., 1990. Frictional-collisional equations of motion for particulate flows and their application to chutes. J. Fluid Mech. 210, 501–535.

Kechagiopoulos, P.N., Voutetakis, S.S., Vasalos, I.A., 2007. Sustainable hydrogen production via reforming of ethylene glycol using a novel spouted bed reactor. Catal. Today 127, 246–255. https://doi.org/10.1016/j.cattod.2007.05.018

Liu, G.-Q., Li, S.-Q., Zhao, X.-L., Yao, Q., 2008. Experimental studies of particle flow dynamics in a two-dimensional spouted bed. Chem. Eng. Sci. 63, 1131–1141. https://doi.org/10.1016/J.CES.2007.11.013

Lun C.K.K., Savage S.B., Jeffrey D.J., C.N., 1984. Kinetic theories for granular flow: inelastic particles in Couette flow and slightly inelastic particles in a general flowfieldNo Title. J. Fluid Mech. 140, 223–256.

M. Syamlal, W. Rogers, and O.T.J., 1993. MFIX Documentation: Volume 1, Theory Guide., in: National Technical Information Service. Springfield VA. https://doi.org/DOE/METC-9411004,

NTIS/DE9400087.

M.V.C. Machado, S.M. Nascimento, C.R. Duarte, M.A.S.B., 2017. Boundary conditions effects on the particle dynamic flow in a rotary drum with a single flight. Powder Technol. 311, 341–349.

Makibar, J., Fernandez-Akarregi, A.R., Amutio, M., Lopez, G., Olazar, M., 2015. Performance of a conical spouted bed pilot plant for bio-oil production by poplar flash pyrolysis. Fuel Process. Technol. 137, 283–289. https://doi.org/10.1016/j.fuproc.2015.03.011

Marchelli F., Moliner C., Bosio B., A.E., 2019. A CFD-DEM sensitivity analysis: the case of a pseudo-2D spouted bed. Powder Technol. In press.

Marchelli, F., Bove, D., Moliner, C., Bosio, B., Arato, E., 2017. Discrete element method for the prediction of the onset velocity in a spouted bed. Powder Technol. 321, 119–131. https://doi.org/10.1016/j.powtec.2017.08.032

Mathur, K.B., Epstein, N., 1974. Developments in spouted bed technology. Can. J. Chem. Eng. 52, 129–144. https://doi.org/10.1002/cjce.5450520201

Mathur, K.B., Gishler, P.E., 1955. A technique for contacting gases with coarse solid particles. AIChE J. 1, 157–164. https://doi.org/10.1002/aic.690010205

Moliner, C., Marchelli, F., Bosio, B., Arato, E., 2017. Modelling of spouted and spout-fluid beds: Key for their successful scale up. Energies 10, 38. https://doi.org/10.3390/en10111729

Moliner, C., Marchelli, F., Bosio, B., Arato, E., 2017. Modelling of spouted and spout-fluid beds: Key for their successful scale up. Energies 10. https://doi.org/10.3390/en10111729

Moliner, C., Marchelli, F., Curti, M., Bosio, B., Rovero, G., Arato, E., 2018a. Spouting behaviour of binary mixtures in square-based spouted beds. Particuology. https://doi.org/10.1016/J.PARTIC.2018.01.003

Moliner, C., Marchelli, F., Spanachi, N., Martinez-Felipe, A., Bosio, B., Arato, E., 2018b. CFD simulation of a Spouted Bed: comparison between the Discrete Element Method (DEM) and

the Two Fluid Method (TFM). Chem. Eng. J. 0–1. https://doi.org/10.1016/j.cej.2018.11.164

Mollick, P.K., Venugopalan, R., Roy, M., Rao, P.T., Sathiyamoorthy, D., Sengupta, P., Sharma, G., Basak, C.B., Chakravartty, J.K., 2015. Deposition of diversely textured buffer pyrolytic carbon layer in TRISO coated particle by controlled manipulation of spouted bed hydrodynamics. Chem. Eng. Sci. 128, 44–53. https://doi.org/10.1016/j.ces.2015.01.065

Olazar, M., San Jose, M.J., Penas, F.J., Aguayo, A.T., Bilbao, J., 1993. Stability and hydrodynamics of conical spouted beds with binary mixtures. Ind. Eng. Chem. Res. 32, 2826–2834. https://doi.org/10.1021/ie00023a053

Rong, L.W., ZHAN, J.M., 2010. Improved DEM-CFD model and validation: A conical-base spouted bed simulation study. J. Hydrodyn. 22, 351–359. https://doi.org/10.1016/S1001-6058(09)60064-0

S. Ogawa, A. Umemura, and N.O., 1980. On the Equation of Fully Fluidized Granular Materials. J. Appl. Math. Phys. 31, 483.

S.H. Hosseini, G. Ahmadi, B. S. Razavi, W.Z., 2010. Computational Fluid Dynamic Simulation of Hydrodynamic Behaviour in a Two-Dimensional Conical Spouted Bed. Energy&Fuels 24, 6086–6098.

San José, M.J., Alvarez, S., García, I., Peñas, F.J., 2013. A novel conical combustor for thermal exploitation of vineyard pruning wastes. Fuel 110, 178–184. https://doi.org/10.1016/j.fuel.2012.10.039

San José, M.J., Alvarez, S., Peñas, F.J., García, I., 2014. Thermal exploitation of fruit tree pruning wastes in a novel conical spouted bed combustor. Chem. Eng. J. 238, 227–233. https://doi.org/10.1016/j.cej.2013.09.073

T. Li, J. Grace, X.B., 2010. Study of wall boundary condition in numerical simulations of bubbling fluidized beds. Powder Technol. 203, 447–457.

Yang, J., Breault, R.W., Weber, J.M., Rowan, S.L., 2018. Determination of flow patterns by a novel image analysis technique in a rectangular spouted bed. Powder Technol. 334, 151–162. https://doi.org/10.1016/j.powtec.2018.04.067

Zhao, X.-L.L., Li, S.-Q.Q., Liu, G.-Q.Q., Yao, Q., Marshall, J.-S.S., 2008. DEM simulation of the particle dynamics in two-dimensional spouted beds. Powder Technol. 184, 205–213. https://doi.org/10.1016/j.powtec.2007.11.044

ACKNOWLEDGMENTS

This work was funded through the LIFE LIBERNITRATE project (LIFE16 ENV/ES/000419) in the framework of the LIFE+ funding programme. EA and AMF acknowledge the traineeship Erasmus+ grant for Laura Ong.

Figure 1

Click here to download high resolution image

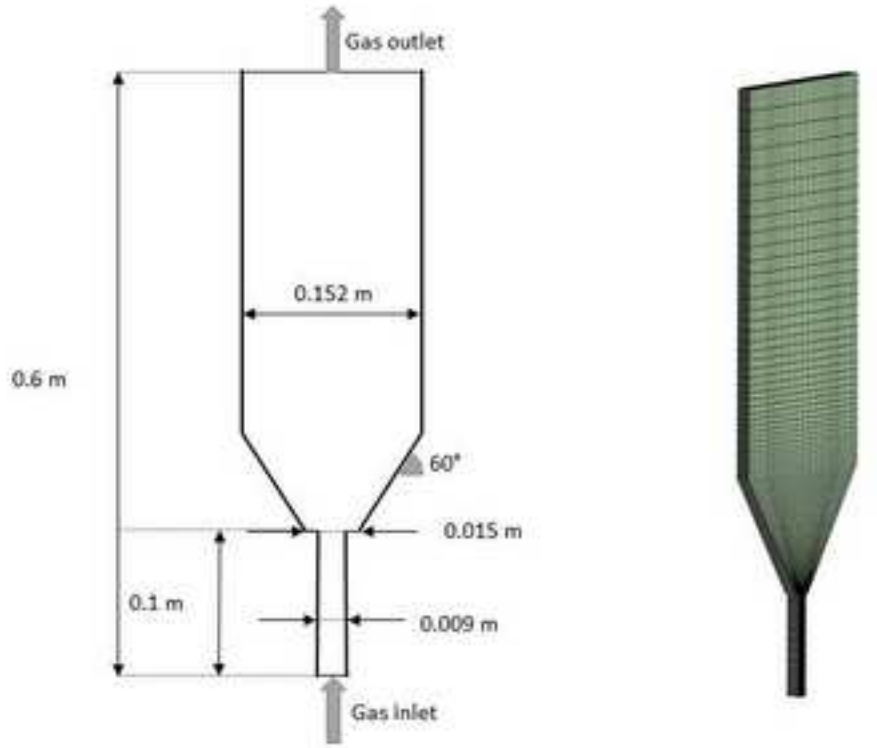

Figure 2

Click here to download high resolution image

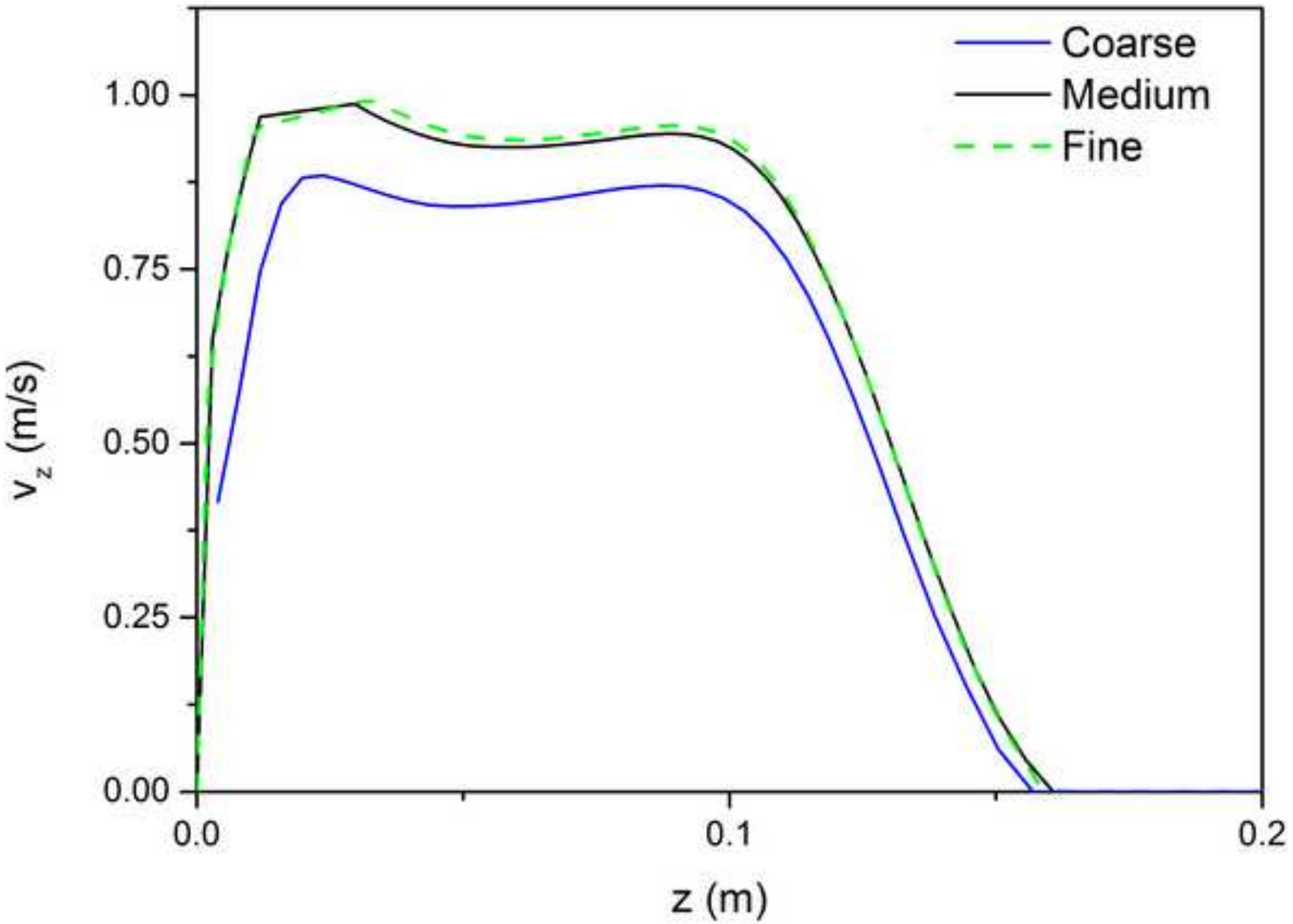

Figure 3
Click here to download high resolution image

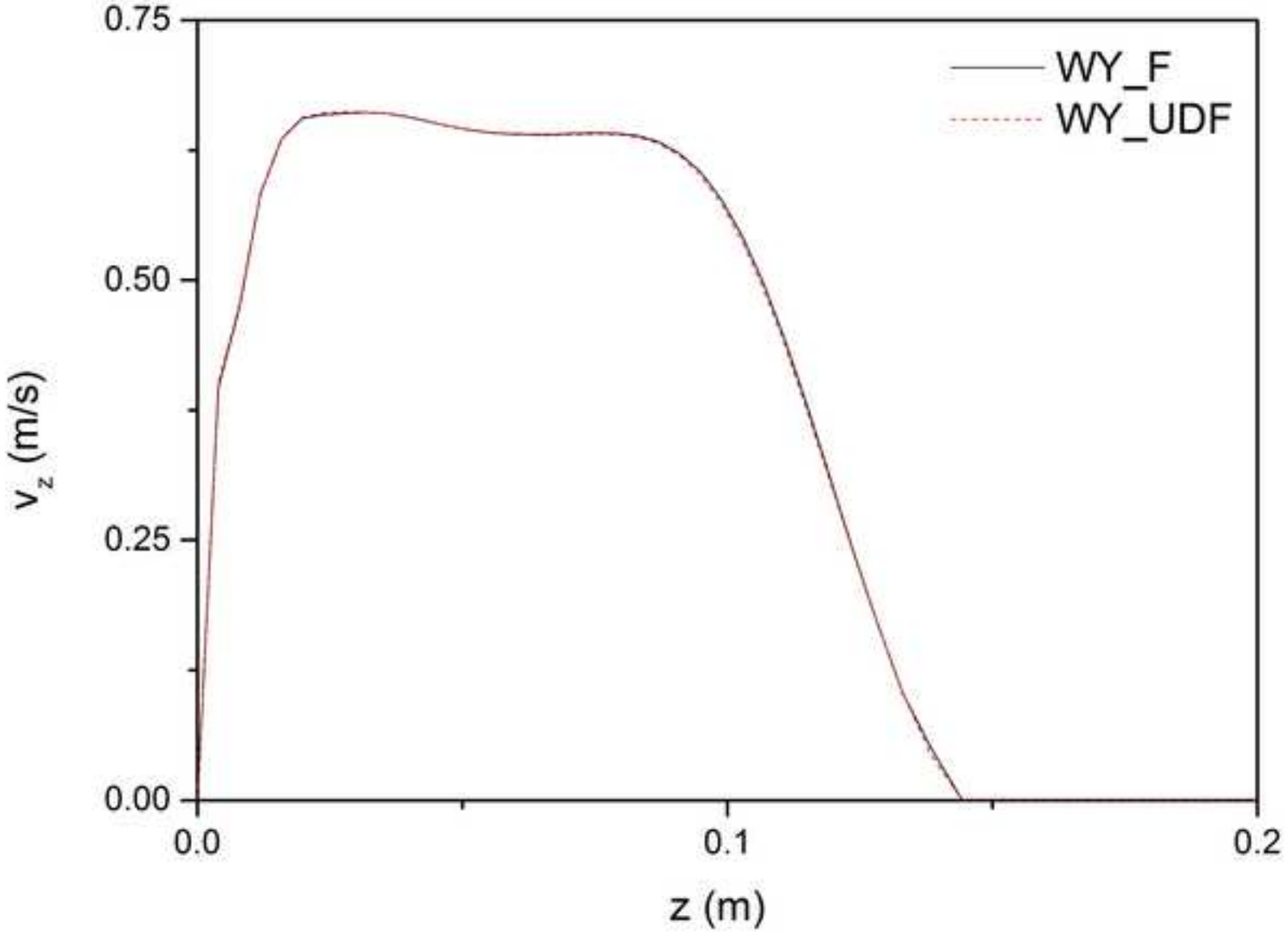

Figure 4

Click here to download high resolution image

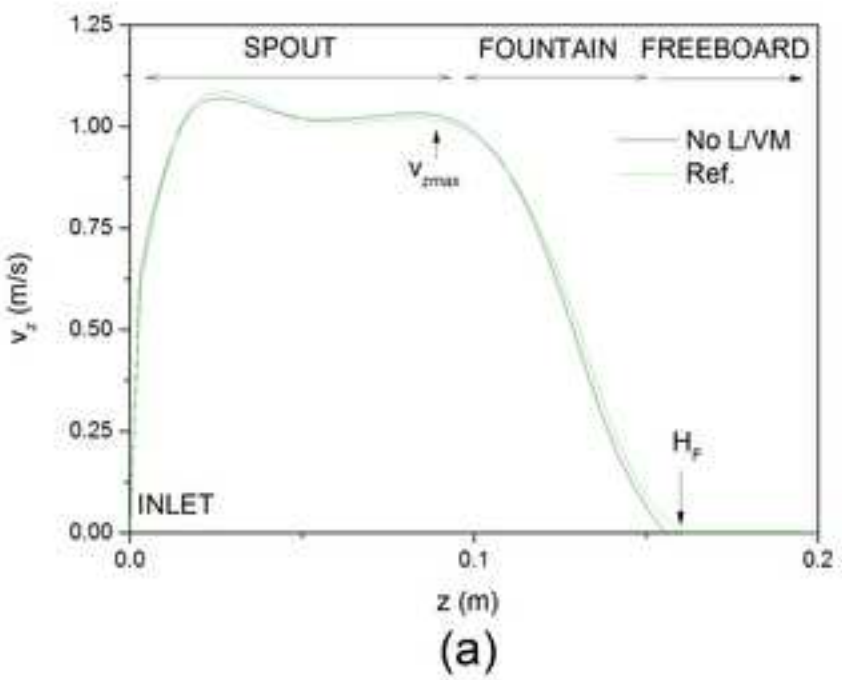

(a)

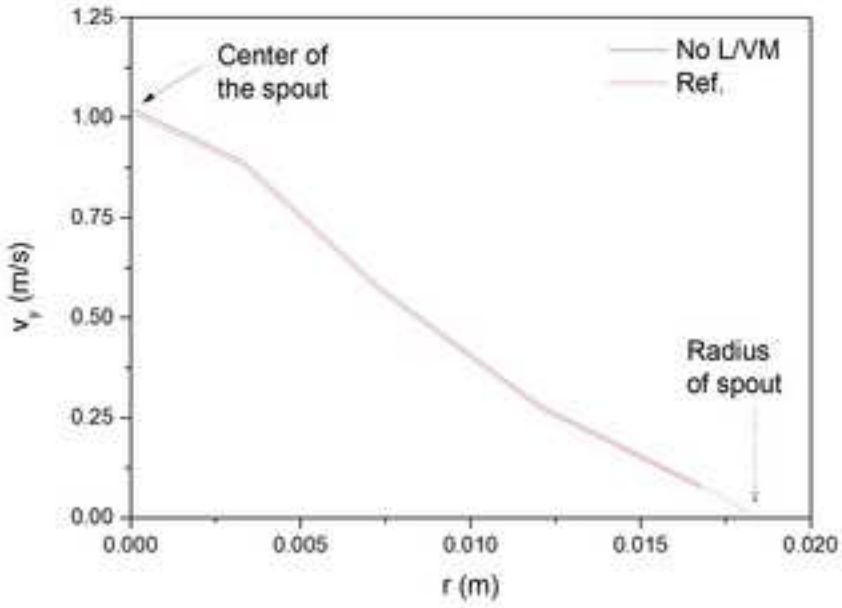

(b)

Figure 5

Click here to download high resolution image

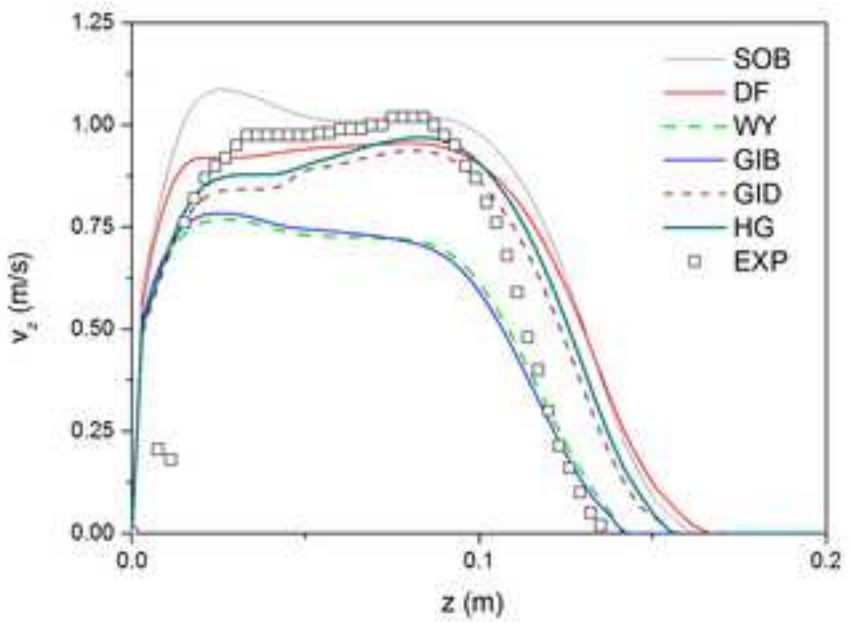

(a)

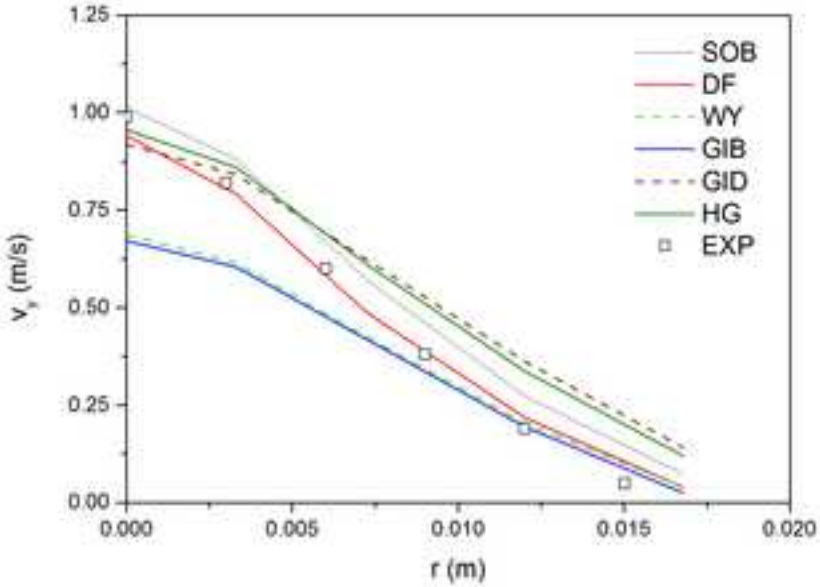

(b)

Figure 6

Click here to download high resolution image

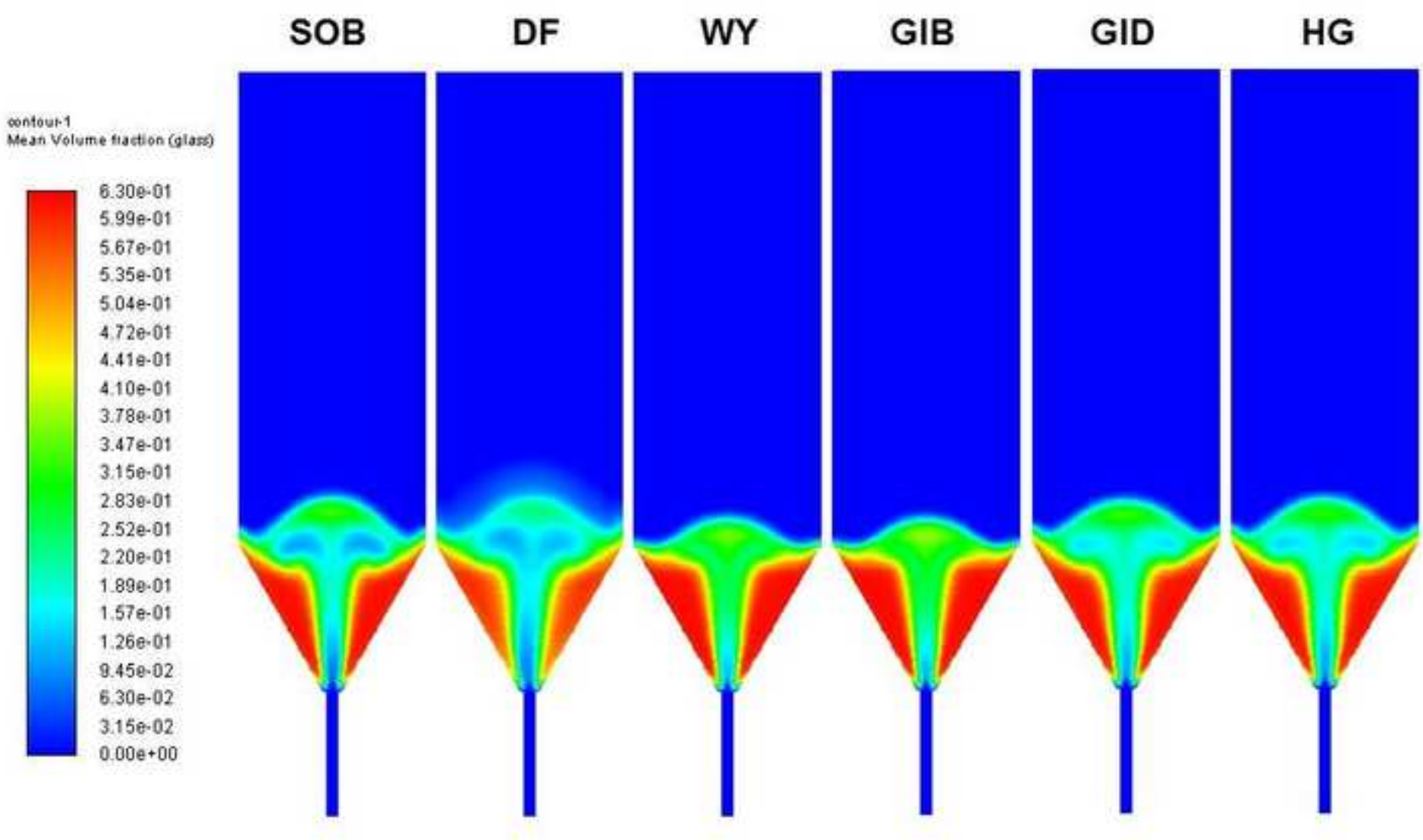

Figure 7

Click here to download high resolution image

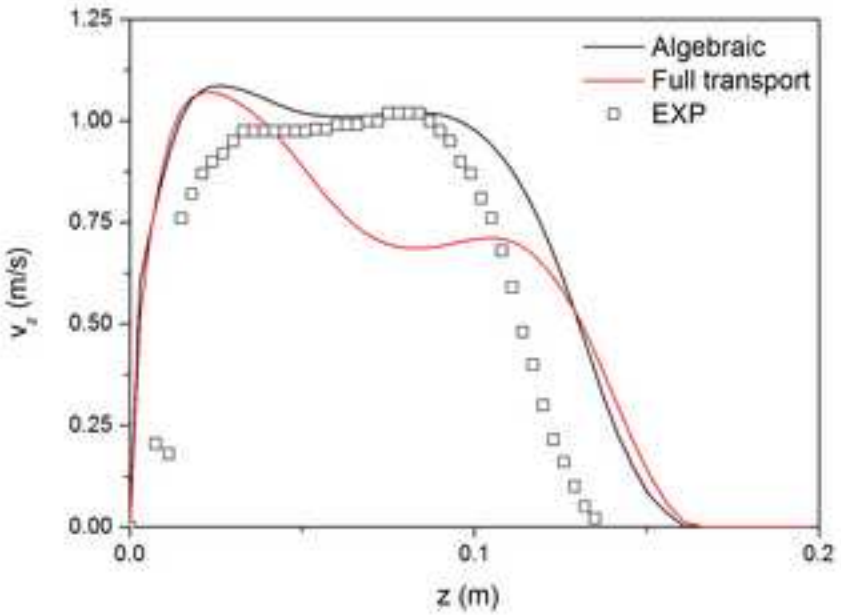

(a)

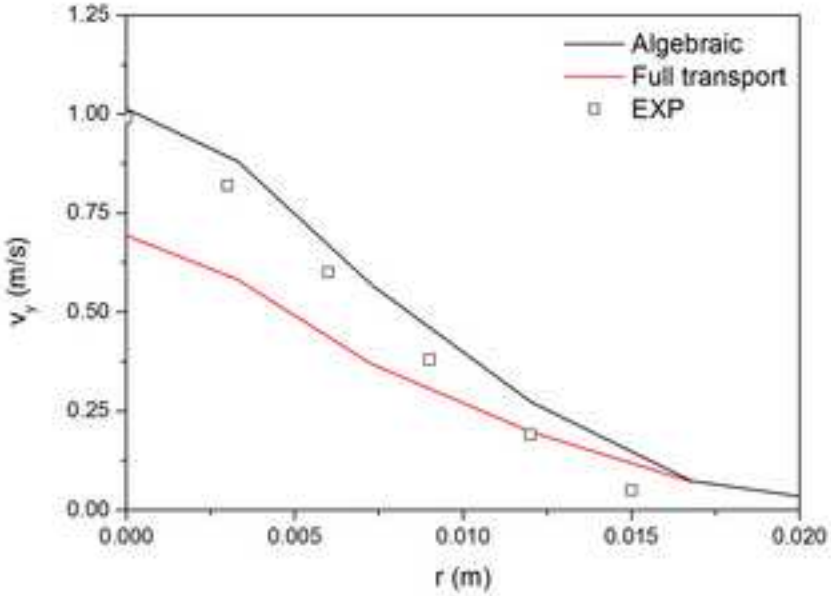

(b)

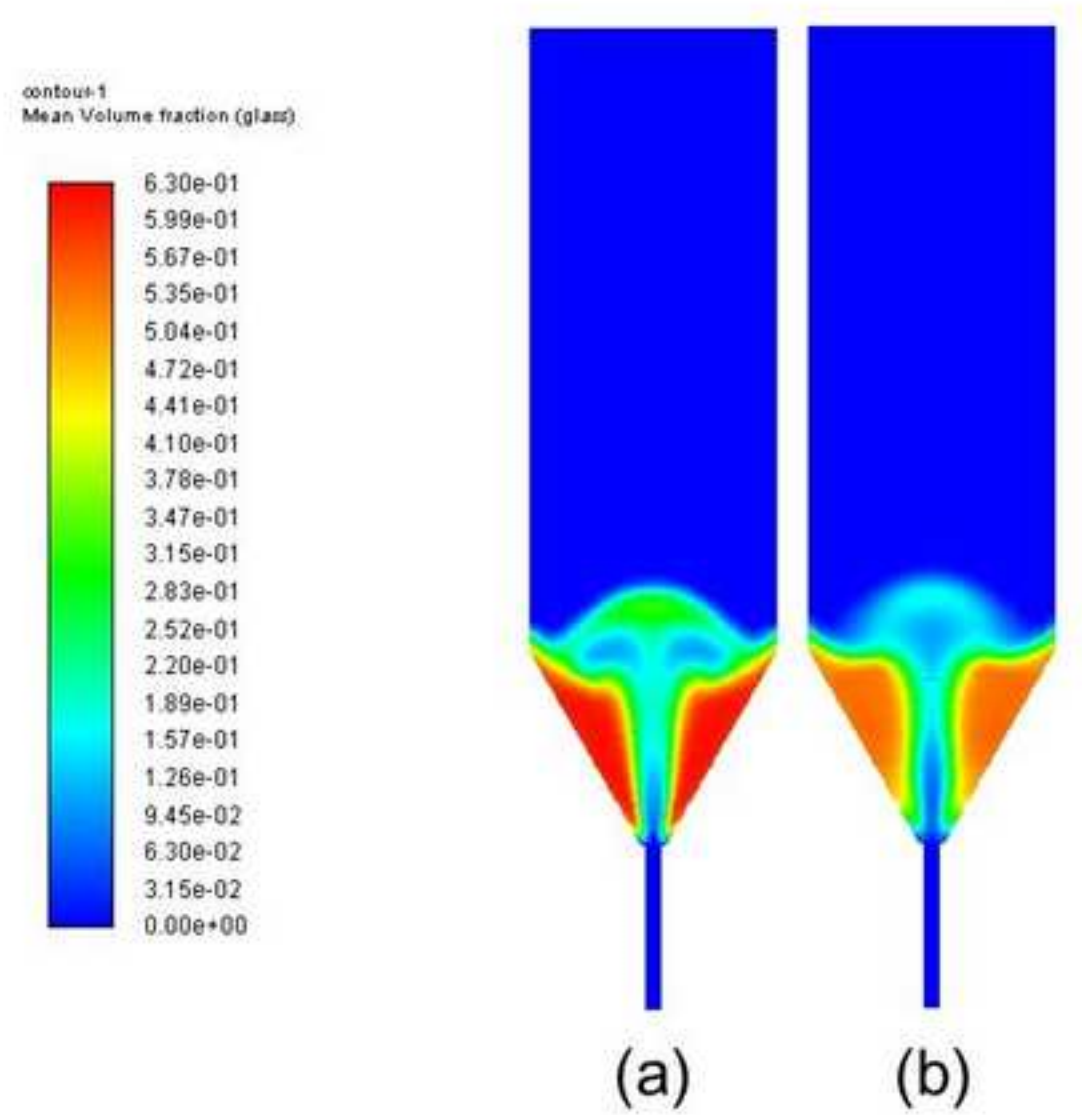

Figure 9

Click here to download high resolution image

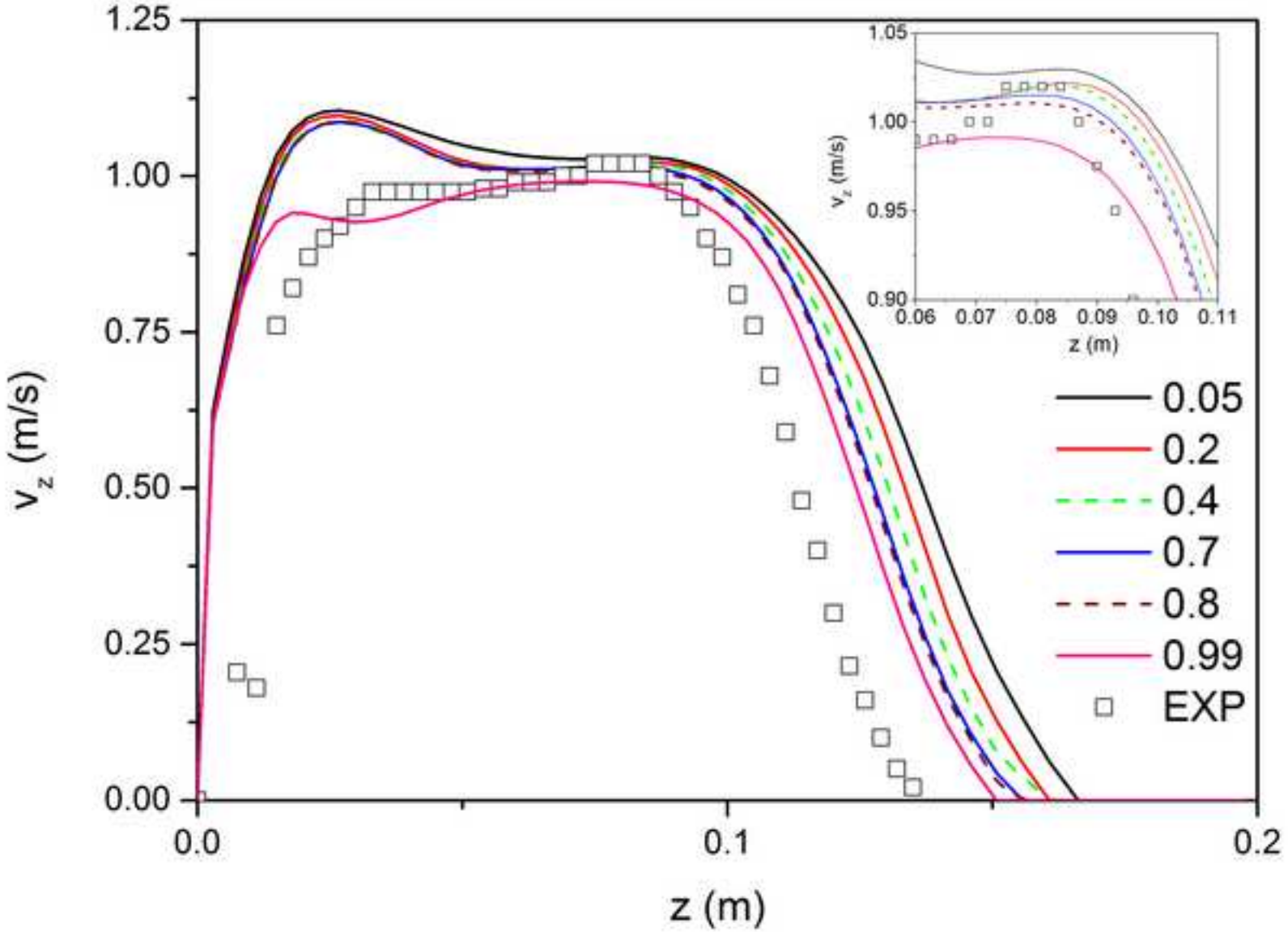

Figure 10

Click here to download high resolution image

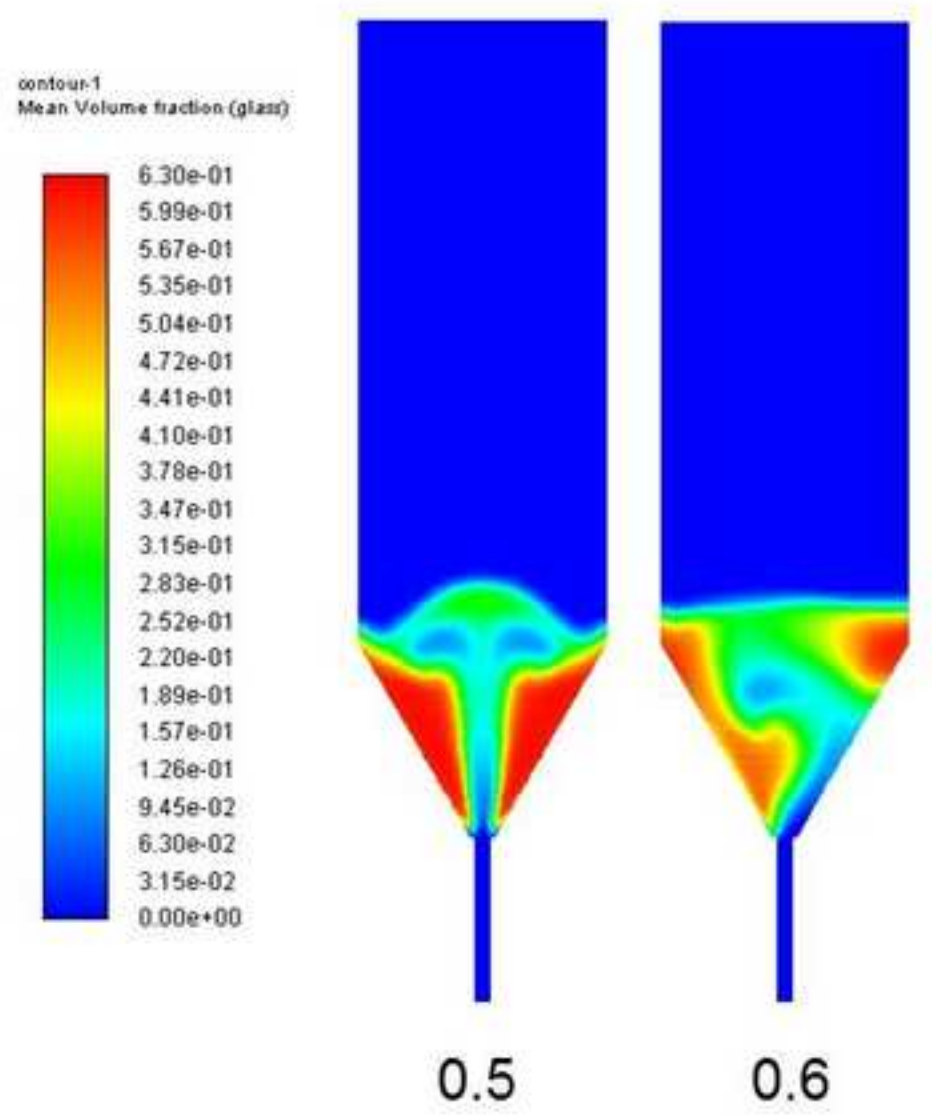

Figure 11

Click here to download high resolution image

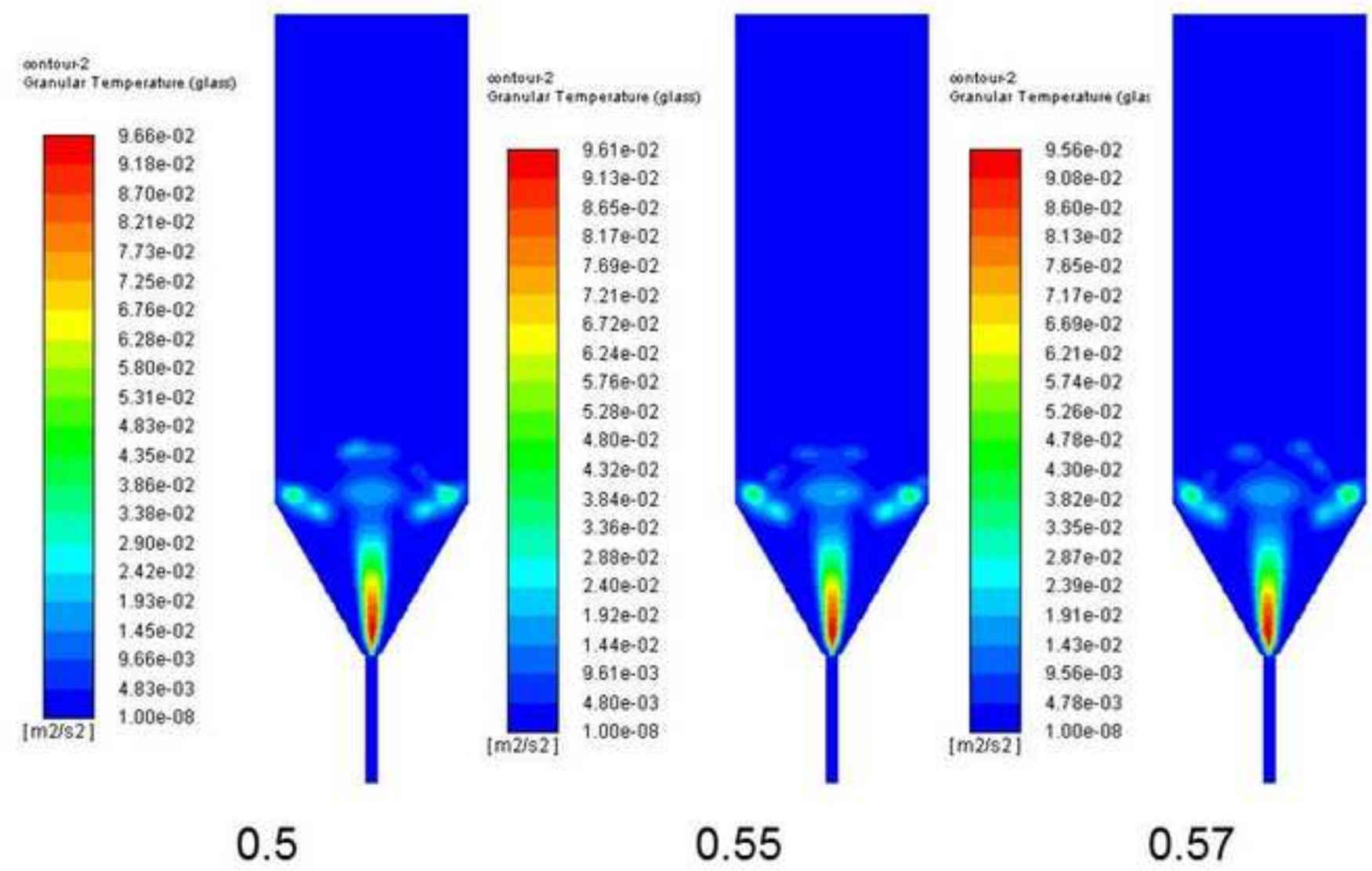

Figure 12

Click here to download high resolution image

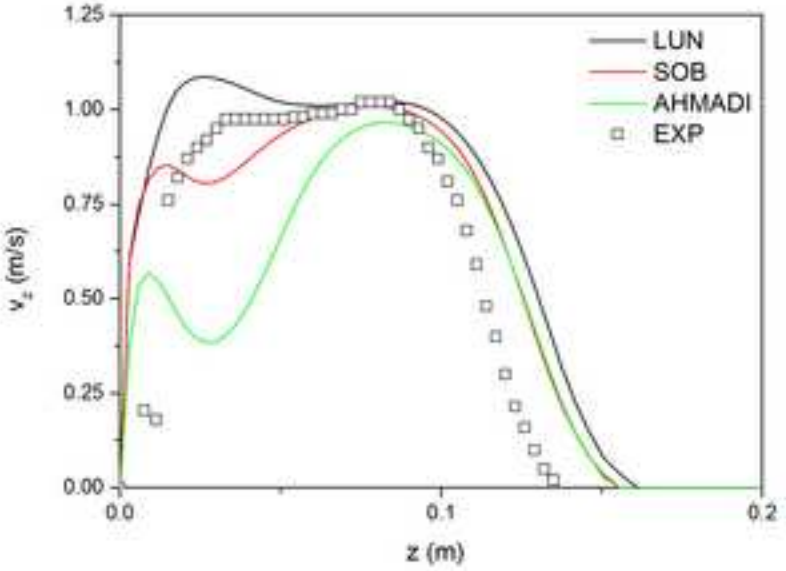

(a)

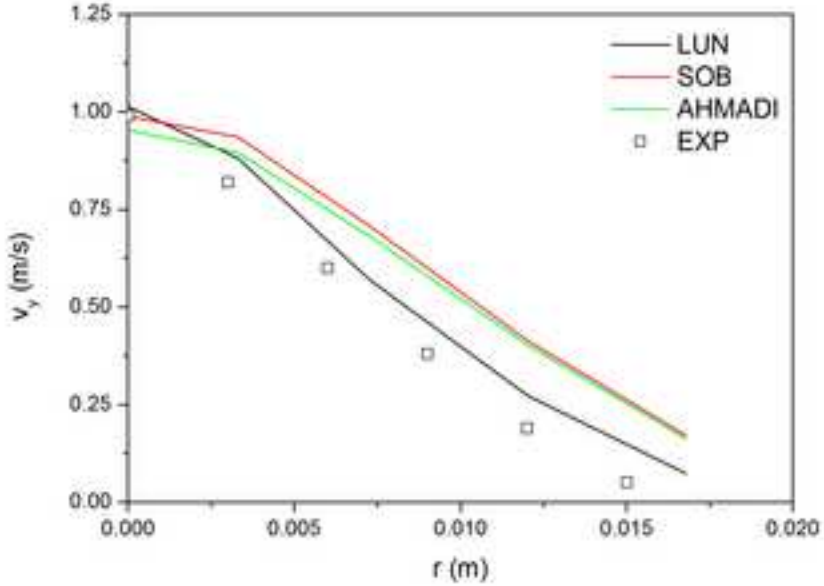

(b)

Figure 13

Click here to download high resolution image

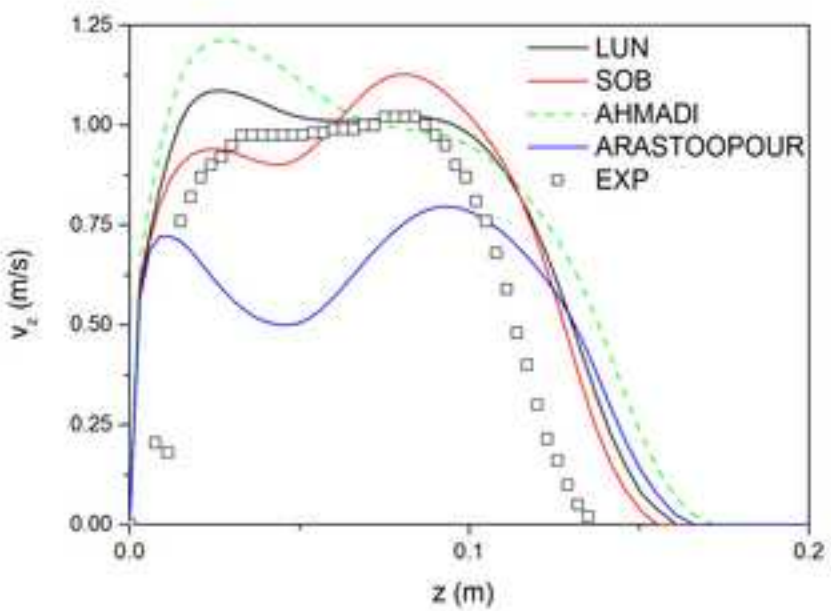

(a)

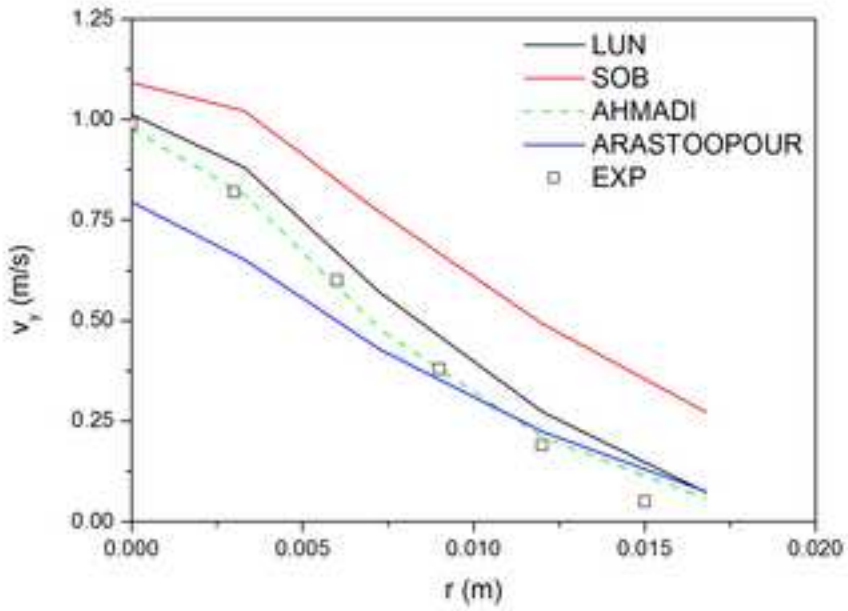

(b)

Figure 14

Click here to download high resolution image

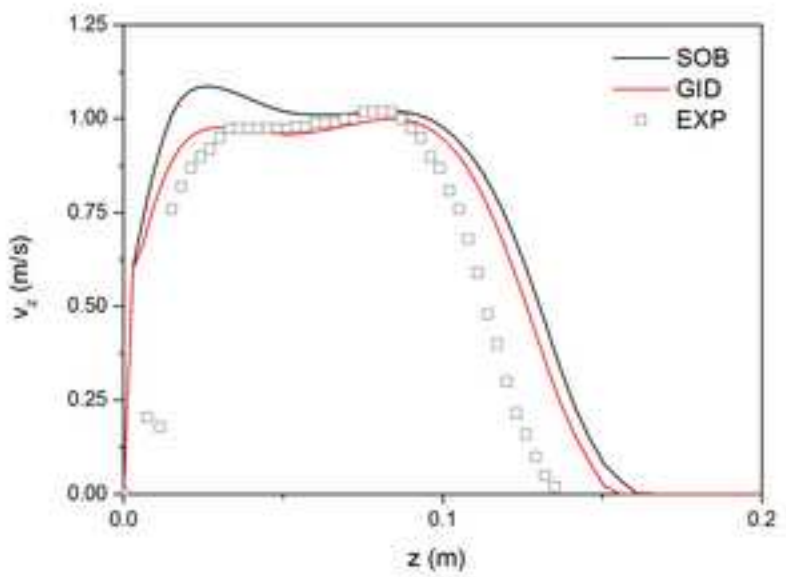

(a)

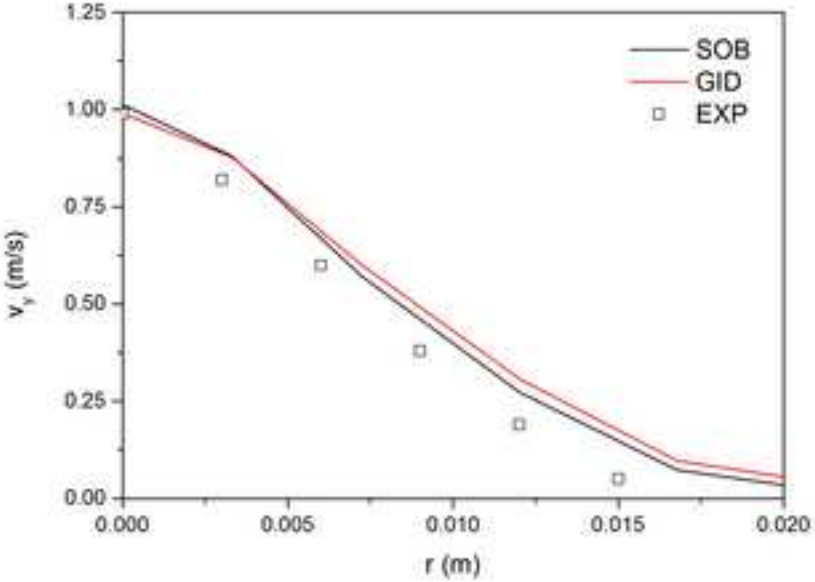

(b)

Figure 15

Click here to download high resolution image

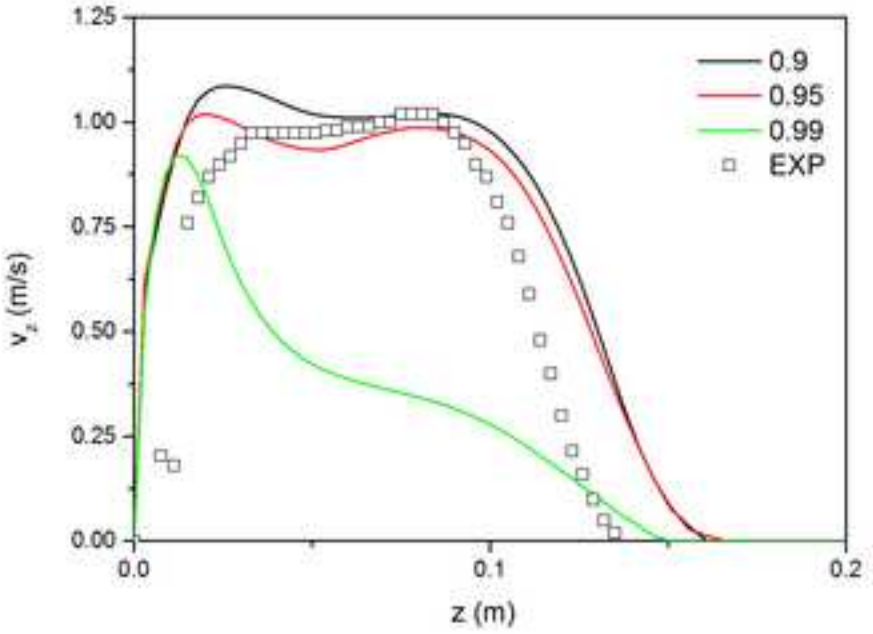

(a)

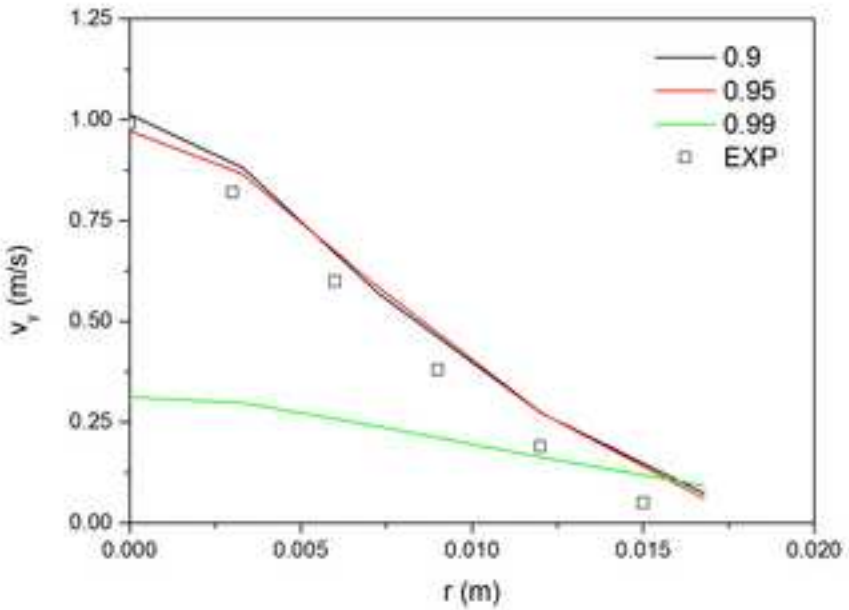

(b)

Figure 16

Click here to download high resolution image

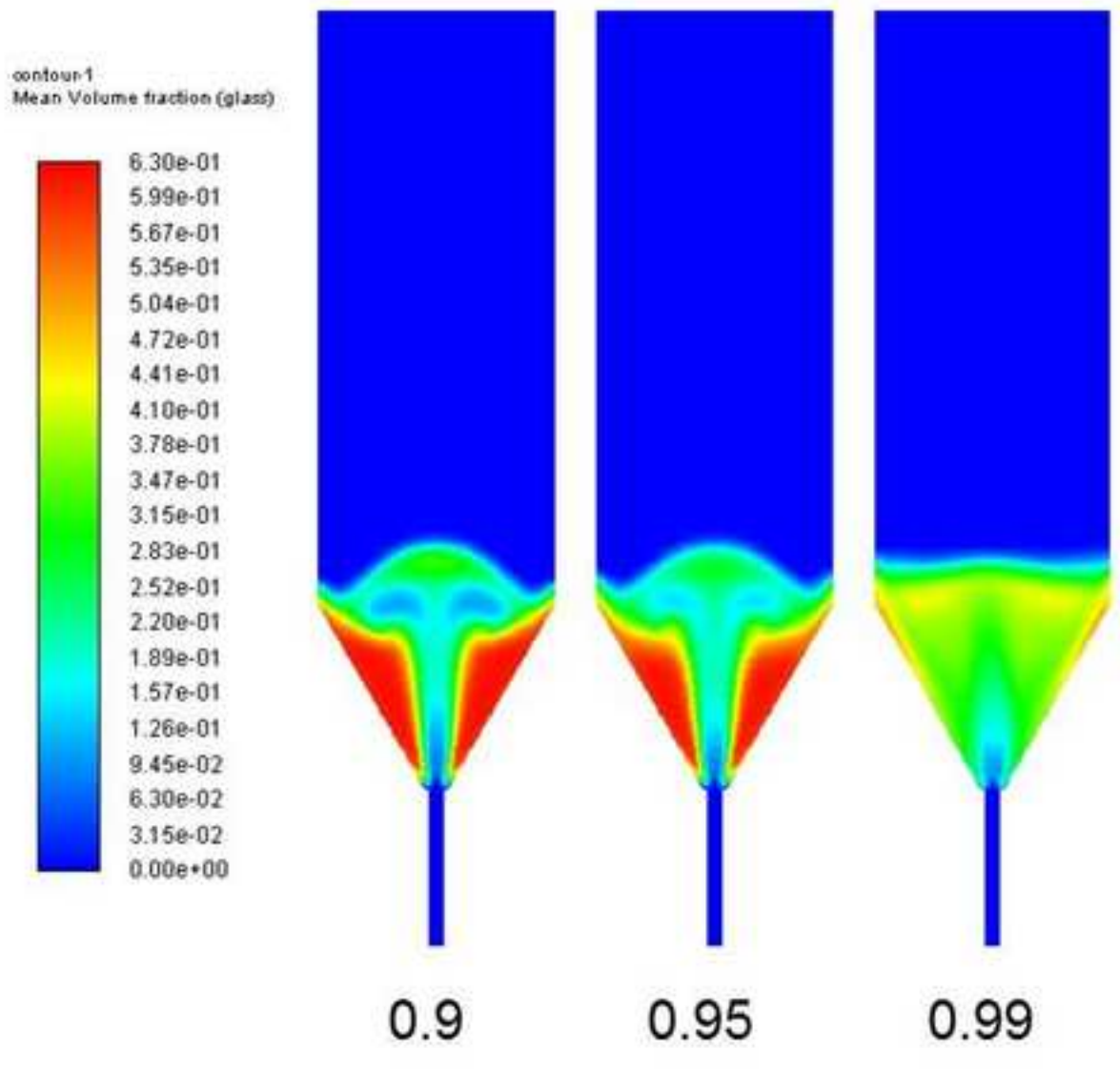

Figure 17

Click here to download high resolution image

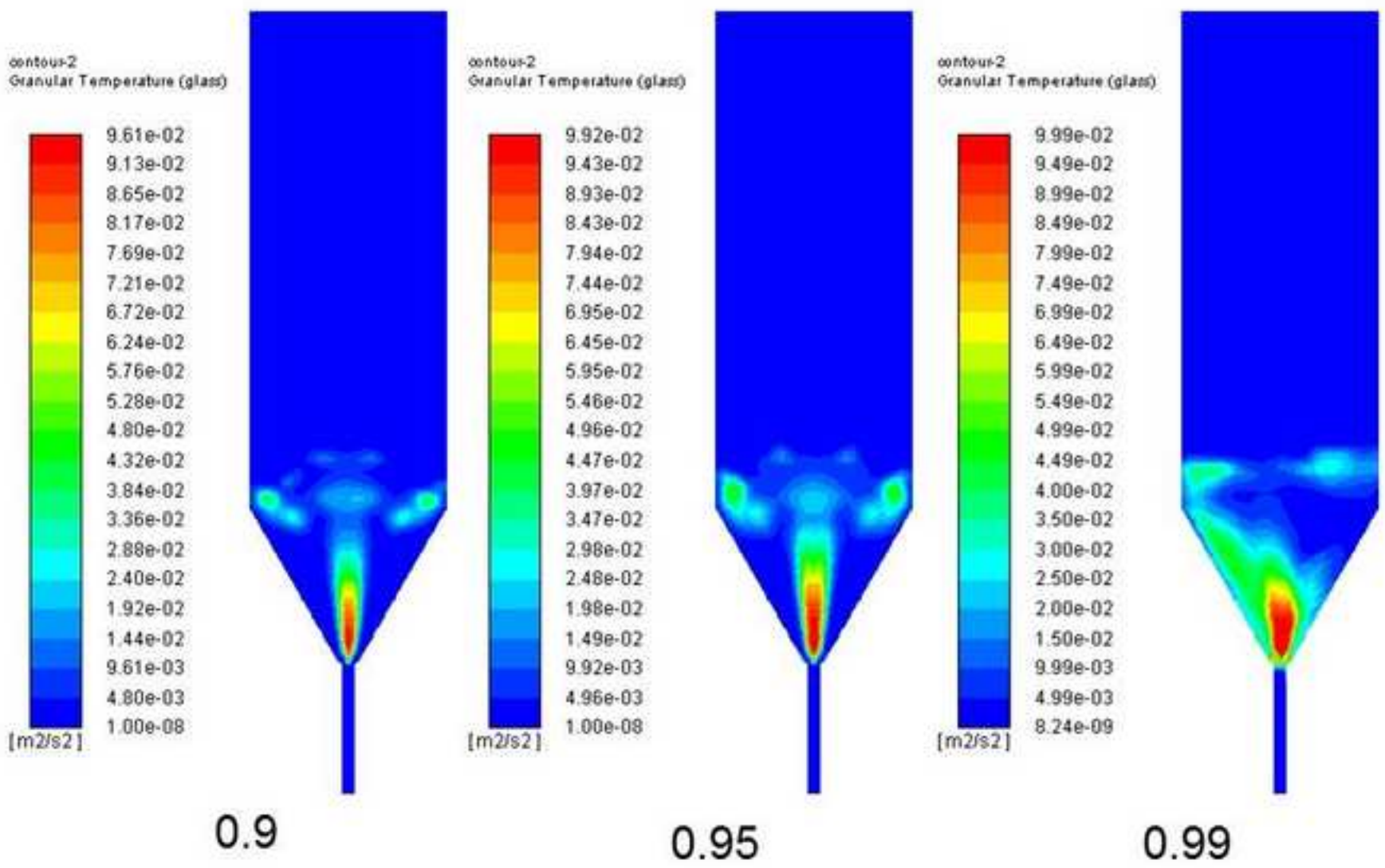

Figure 18

Click here to download high resolution image

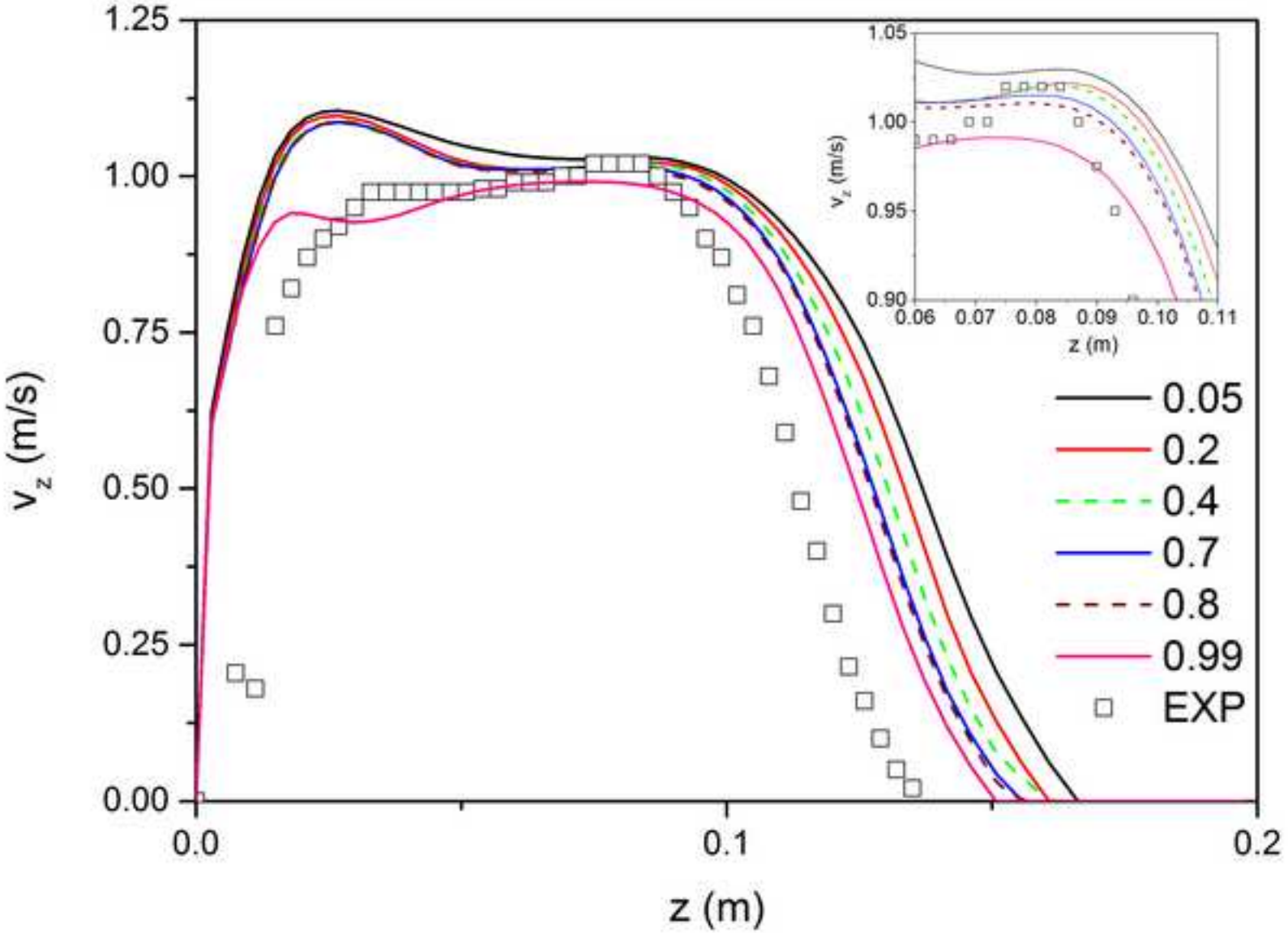

Figure 19

Click here to download high resolution image

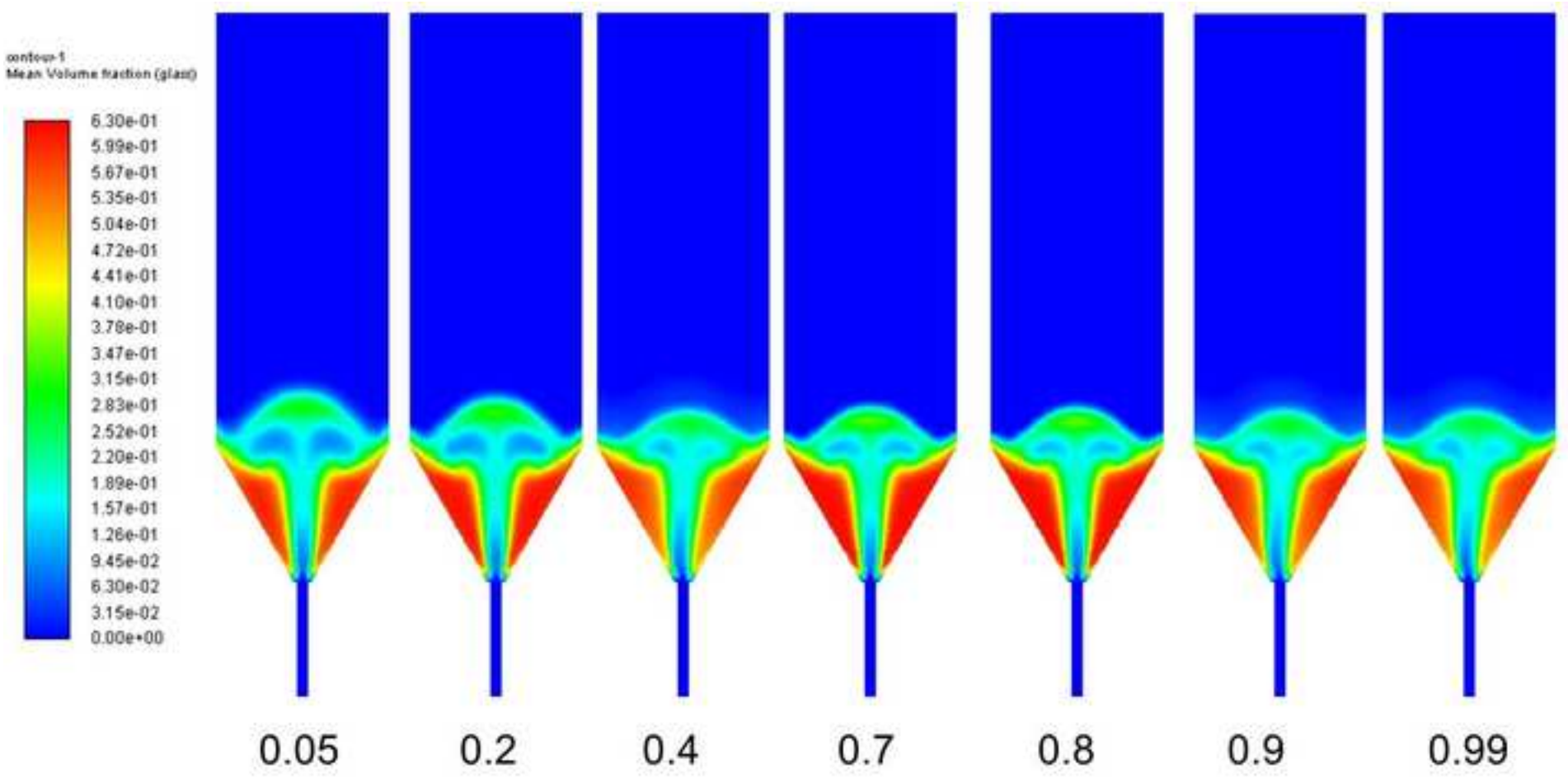

Figure 20

Click here to download high resolution image

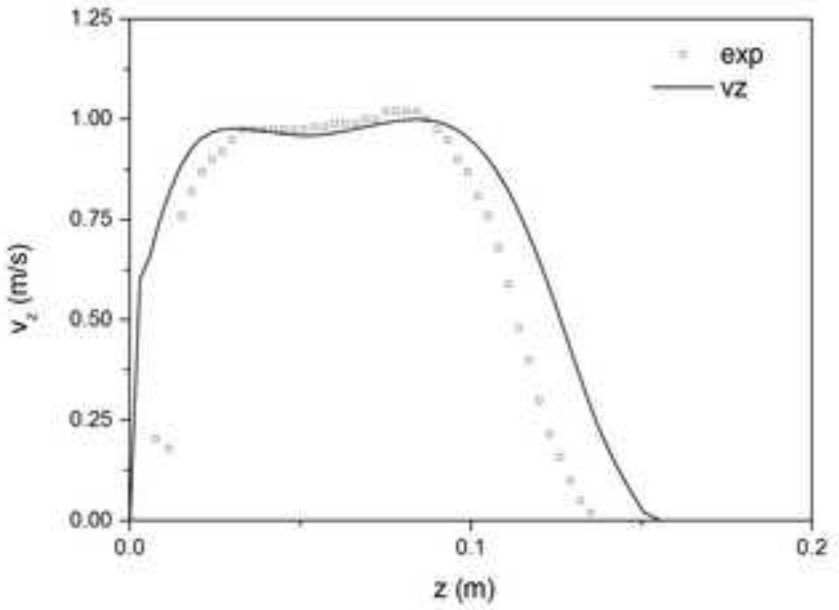

(a)

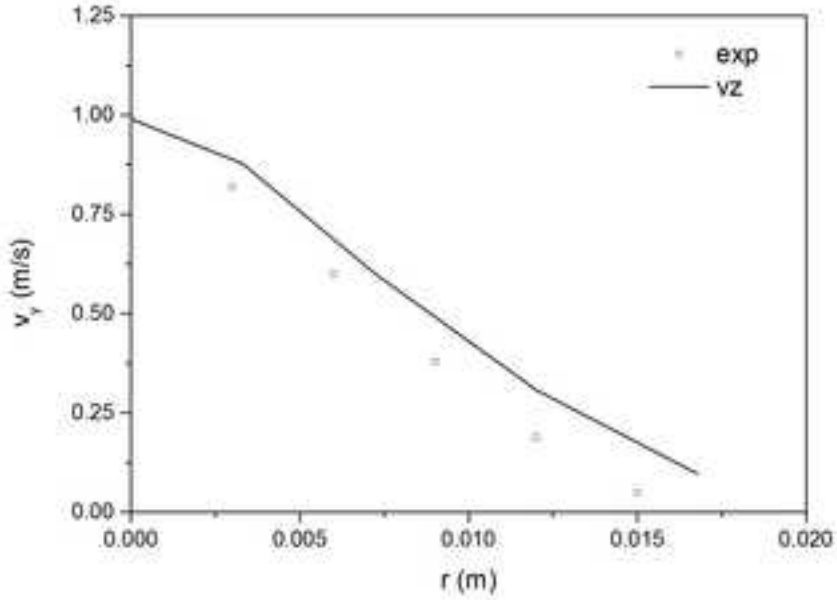

(b)

Figure 21

Click here to download high resolution image

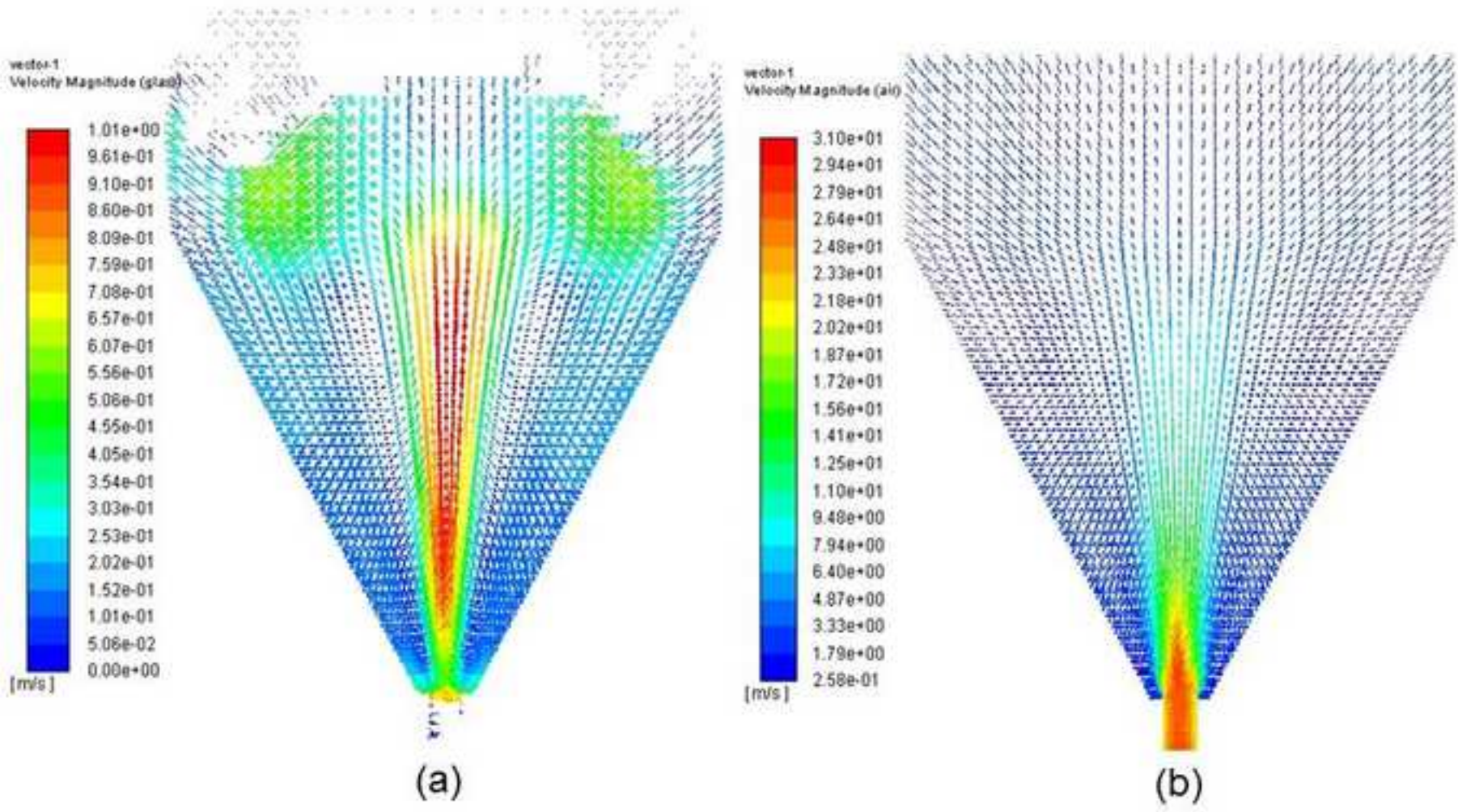

Table 1. Overview of drag functions for fluid-solid interactions available within Fluent 19.1.

Drag Model	**Recommended use**
Wen-Yu (WY)	Thin, dilute systems
Gidaspow (GID)	Dense, compact fluidized beds
Syamlal-O'Brien (SOB)	Dense, compact systems
Huilin-Gidaspow (HG)	Dense, compact fluidized beds
Gibilaro (GIB)	Thin systems

Table 2. Definition of experimental conditions

Parameter	Value	Units
Air density (ρ_g)	1.225	kg/m^3
Air viscosity (μ_g)	1.7894 ·10^{-5}	Pa/s
Glass beads density (ρ_s)	2380	kg/m^3
Glass beads diameter (d_s)	0.00203	m
Shape of particles	Spherical	-

Table 3. Initial reference parameters and tested options for all the varied parameters

Parameter	Reference	Tested options
Drag Law (DL)	Syamlal O'Brien	Gidaspow, Gibilaro, Wen-Yu, Huilin-Gidaspow, Di Felice
Granular temperature (Θ_s)	Algebraic	Full transport equation
Friction Packing Limit (FPL)	0.55	0.5, 0.57, 0.6
Solids Pressure (p_s)	Lun	Syamlal O'Brien, Ahmadi
Radial Distribution (g_0)	Lun	Syamlal O'Brien, Ahmadi, Arastoopour
Granular Viscosity (GV)	Syamlal O'Brien	Gidaspow
Restitution Coefficient (e_{ss})	0.9	0.95, 0.99
Specularity Coefficient (φ)	0.4	0.05, 0.2, 0.7, 0.8, 0.99

Table 4. Simulation results and error (with respect to experimental data) for different DL.

DL	v_{zmax} (m/s)	$Error_1$ (%)	H_F (m)	$Error_2$ (%)
SOB	1,017	0,4	0,159	17,8
DF	0,944	6,8	0,164	21,5
WY	0,719	29,0	0,141	4,4
GIB	0,719	29,0	0,141	4,4
GID	0,932	8.0	0,155	14,1
HG	0,965	4,7	0,155	14,8

Table 5. Simulated results and error with respect to experimental data for the tested p_s

p_s	v_{zmax} (m/s)	Error (%)	H_F (m)	Error (%)
LUN	1.028	1.48	0.160	18.52
SOB	1.022	0.93	0.153	13.33
AHMADI	0.972	4.05	0.153	13.33

Table 6. Simulated results and error with respect to experimental data for the tested g_0

g_0	v_{zmax} (m/s)	Error (%)	H_F (m)	Error (%)
LUN	1.016	1.48	0.159	17.78
SOB	1.130	11.55	0.155	14.81
AHMADI	0.987	2.57	0.165	22.22
ARASTOOPUR	0.794	21.62	0.171	26.67

Table 7. Simulated results and error with respect to experimental data for the tested e_{ss}

e_{ss}	v_{zmax} (m/s)	Error (%)	H_F (m)	Error (%)
0.90	1.022	0.88	0.161	19.26
0.95	0.992	2.07	0.155	14.81
0.99	*0.922*	*8.98*	*0.149*	*10.37*

Table 8. Simulated results and error with respect to experimental data for the tested φ.

φ	v_{zmax} (m/s)	Error (%)	H_F (m)	Error (%)
0.05	1.032	1.88	0.165	22.22
0.20	1.019	0.59	0.160	18.52
0.40	1.017	0.39	0.160	18.52
0.70	1.012	0.10	0.154	14.07
0.80	1.006	0.69	0.154	14.07
0.99	0.993	1.97	0.150	11.11

Highlights

- We simulated a literature pseudo-2D spouted bed employing the CFD-TFM approach in Ansys Fluent 19.1
- We performed an extensive sensitivity analysis based on various sub-models and parameters
- Drag force and the definition of the granular phase have the greatest impact
- We included Di Felice's drag law through a User-Defined Function
- Based on the sensitivity analysis we optimized our model

Declaration of interests

☒ The authors declare that they have no known competing financial interests or personal relationships that could have appeared to influence the work reported in this paper.

☐The authors declare the following financial interests/personal relationships which may be considered as potential competing interests: